

Neural Networks

Personalised Predictive Modelling with Spiking Neural Networks of Longitudinal MRI Neuroimaging Cohort --Manuscript Draft--

Manuscript Number:	
Article Type:	Article
Section/Category:	Learning Systems
Keywords:	Personalised modelling; spiking neural networks; longitudinal MRI data; dementia; classification; prediction.
Corresponding Author:	Maryam Doborjeh, PhD, Lecturer Auckland University of Technology Auckland, NEW ZEALAND
First Author:	Maryam Doborjeh, PhD, Lecturer
Order of Authors:	Maryam Doborjeh, PhD, Lecturer
	Zohreh Doborjeh, PhD, Research Fellow
	Alexander Merkin, PhD, Research Fellow
	Helena Bahrami, PhD Student
	Alexander Sumich
	Rita Krishnamurthi, A/Professor
	Oleg N Medvedev, PhD, Lecturer
	Mark Crook-Rumsey, PhD
	Catherine Morgan, PhD, Research Fellow
	Ian Kirk, PhD
	Perminder Sachdev, PhD
	Henry Brodaty
	Kristan Kang, PhD
	Wei Wen
	Valery Feigin, PhD, Professor
	Nikola Kasabov, PhD, Professor
Abstract:	<p>Background : Longitudinal neuroimaging provides spatiotemporal brain data (STBD) measurement that can be utilised to understanding dynamic changes in brain structure and/or function underpinning cognitive activities. Making sense of such highly interactive information is challenging, given that the features manifest intricate temporal, causal relations between the spatially distributed neural sources in the brain.</p> <p>Methods : The current paper argues for the advancement of deep learning algorithms in brain-inspired spiking neural networks (SNN), capable of modelling structural data across time (longitudinal measurement) and space (anatomical components). The paper proposes a methodology and a computational architecture based on SNN for building personalised predictive models from longitudinal brain data to accurately detect, understand, and predict the dynamics of an individual's functional brain state. The pipeline methodology includes methods for clustering, data interpolation, deep learning in a 3-dimensional brain-template structured SNN model, classification and prediction of outcomes, visualisation of structural brain changes related to predicted outcomes, interpretation of results, and individual and group predictive marker discovery.</p> <p>Results : To demonstrate the functionality of the proposed methodology, the paper presents experimental results on a longitudinal magnetic resonance imaging (MRI) dataset derived from 175 older adults of the internationally recognised community-based cohort Sydney Memory and Ageing Study (MAS) spanning 6 years</p>

	<p>of follow-up. Significance : The models were able to accurately classify and predict 2 years ahead of cognitive declines, such as mild cognitive impairment (MCI) and dementia with 95% and 91% accuracy, respectively. The proposed methodology also offers a 3-dimensional visualisation of the MRI models reflecting the dynamic patterns of regional changes in white matter hyperintensity (WMH) and brain volume over 6 years. Conclusion : The results suggest predictive markers amongst explored brain patterns for dementia and MCI. The proposed method is a generic one, applicable to other longitudinal data sets such as other neuroimaging modalities, including also demographic, genetic, and clinical data.</p>
Suggested Reviewers:	<p>Hamid Abbasi, PhD Research Fellow, The University of Auckland h.abbasi@auckland.ac.nz Hamid's area of research is neural networks for brain data modelling.</p>
	<p>Hideaki Kawano, PhD A/Professor, Kyushu Institute of Technology kawano@ecs.kyutech.ac.jp</p>
	<p>Enmei Tu, PhD A/Professor, Shanghai Jiao Tong University Medical Library: Shanghai Jiao Tong University School of Medicine tuen@sjtu.edu.cn</p>
	<p>Wilson Goh Wen Bin, PhD Lecturer, Nanyang Technological University - Jurong Campus: Nanyang Technological University wilsongoh@ntu.edu.sg</p>

Highlights

- New personalised modelling methodology for modelling of longitudinal MRI data to predict cognitive outcome.
- Biologically inspired spiking neural networks for modelling of integrated spatial and temporal components of longitudinal MRI data.
- 3D brain-shaped visualisation of the changes in MRI anatomical components over 6 years.
- Spike-time dependent learning rules (supervised and unsupervised) in personalised spiking neural networks.
- Personalised profiling of an individual to improve interpretability.

Title Page

Title: Personalised Predictive Modelling with Spiking Neural Networks of Longitudinal MRI Neuroimaging Cohort

Authors Names:

- Maryam Doborjeh, Information Technology and Software Engineering Department, Auckland University of Technology, Auckland 1010, New Zealand
- Zohreh Doborjeh, Department of Audiology, School of Population Health, Faculty of Medical and Health Sciences, The University of Auckland, New Zealand
- Alexander Merkin, Faculty of Health & Environmental Sciences, National Institute for Stroke and Applied Neurosciences, Auckland University of Technology, Private Bag 92006, Auckland 1142, New Zealand
- Helena Bahrami, School of Engineering, Computer and Mathematical Sciences, Auckland University of Technology, Auckland 1010, New Zealand
- Alexander Sumich, Division of Psychology, Nottingham Trent University, Nottingham, United Kingdom
- Rita Krishnamurthi, Faculty of Health & Environmental Sciences, National Institute for Stroke and Applied Neurosciences, Auckland University of Technology, Private Bag 92006, Auckland 1142, New Zealand
- Oleg N. Medvedev, University of Waikato, School of Psychology, Hamilton, New Zealand
- Mark Crook-Rumsey, Division of Psychology, Nottingham Trent University, Nottingham, United Kingdom
- Catherine Morgan, School of Psychology and Centre for Brain Research, University of Auckland, New Zealand; and Brain Research New Zealand, New Zealand
- Ian Kirk, School of Psychology and Centre for Brain Research, University of Auckland, New Zealand; and Brain Research New Zealand, New Zealand
- Perminder Sachdev, Centre for Healthy Brain Ageing (CHeBA), School of Psychiatry, University of New South Wales, Sydney, Australia; and Neuropsychiatric Institute, the Prince of Wales Hospital, Sydney, Australia
- Henry Brodaty, Centre for Healthy Brain Ageing (CHeBA), School of Psychiatry, University of New South Wales, Sydney, Australia
- Kristan Kang, Centre for Healthy Brain Ageing (CHeBA), School of Psychiatry, University of New South Wales, Sydney, Australia
- Wei Wen, Centre for Healthy Brain Ageing (CHeBA), School of Psychiatry, University of New South Wales, Sydney, Australia
- Valery Feigin, Faculty of Health & Environmental Sciences, National Institute for Stroke and Applied Neurosciences, Auckland University of Technology, Private Bag 92006, Auckland 1142, New Zealand; and Research Center of Neurology, Moscow, Russia
- Nikola Kasabov, School of Engineering, Computer and Mathematical Sciences, Auckland University of Technology, New Zealand; and George Moore Chair, Ulster University, Londonderry, United Kingdom

Contact persons: Maryam Doborjeh, mgholami@aut.ac.nz

Personalised Predictive Modelling with Spiking Neural Networks of Longitudinal MRI Neuroimaging Cohort

Maryam Doborjeh^{1*}, Zohreh Doborjeh², Alexander Merkin³, Helena Bahrami⁴, Alexander Sumich⁵, Rita Krishnamurthi³, Oleg N. Medvedev⁶, Mark Crook-Rumsey^{5,4}, Catherine Morgan^{7,8}, Ian Kirk^{7,8}, Perminder Sachdev^{9,10}, Henry Brodaty⁹, Kristan Kang⁹, Wei Wen⁹, Valery Feigin^{3,11}, Nikola Kasabov^{4,12}

¹Information Technology and Software Engineering Department, Auckland University of Technology, New Zealand

²Department of Audiology, School of Population Health, Faculty of Medical and Health Sciences | The University of Auckland, New Zealand

³Faculty of Health & Environmental Sciences, National Institute for Stroke and Applied Neurosciences, Auckland University of Technology, Private Bag 92006, Auckland 1142, New Zealand

⁴School of Engineering, Computer and Mathematical Sciences, Auckland University of Technology, New Zealand

⁵Division of Psychology, Nottingham Trent University, Nottingham, United Kingdom

⁶University of Waikato, School of Psychology, Hamilton, New Zealand

⁷School of Psychology and Centre for Brain Research, University of Auckland, New Zealand

⁸Brain Research New Zealand, New Zealand

⁹Centre for Healthy Brain Ageing (CHeBA), School of Psychiatry, University of New South Wales, Sydney, Australia

¹⁰Neuropsychiatric Institute, the Prince of Wales Hospital, Sydney, Australia

¹¹Research Center of Neurology, Moscow, Russia

¹²George Moore Chair, Ulster University, Londonderry, United Kingdom

*contact persons: mgholami@aut.ac.nz

Abstract. *Background:* Longitudinal neuroimaging provides spatiotemporal brain data (STBD) measurement that can be utilised to understanding dynamic changes in brain structure and/or function underpinning cognitive activities. Making sense of such highly interactive information is challenging, given that the features manifest intricate temporal, causal relations between the spatially distributed neural sources in the brain. *Methods:* The current paper argues for the advancement of deep learning algorithms in brain-inspired spiking neural networks (SNN), capable of modelling structural data across time (longitudinal measurement) and space (anatomical components). The paper proposes a methodology and a computational architecture based on SNN for building personalised predictive models from longitudinal brain data to accurately detect, understand, and predict the dynamics of an individual's functional brain state. The pipeline methodology includes methods for clustering, data interpolation, deep learning in a 3-dimensional brain-template structured SNN model, classification and prediction of outcomes, visualisation of structural brain changes related to predicted outcomes, interpretation of results, and individual and group predictive marker discovery. *Results:* To demonstrate the functionality of the proposed methodology, the paper presents experimental results on a longitudinal magnetic resonance imaging (MRI) dataset derived from 175 older adults of the internationally recognised community-based cohort Sydney Memory and Ageing Study (MAS) spanning 6 years of follow-up. *Significance:* The models were able to accurately classify and predict 2 years ahead of cognitive declines, such as mild cognitive impairment (MCI) and dementia with 95% and 91% accuracy, respectively. The proposed methodology also offers a 3-dimensional visualisation of the MRI models reflecting the dynamic patterns of regional changes in white matter hyperintensity (WMH) and brain volume over 6 years. *Conclusion:* The results suggest predictive markers amongst explored brain patterns for dementia and MCI. The proposed method is a generic one, applicable to other longitudinal data sets such as other neuroimaging modalities, including also demographic, genetic, and clinical data.

Keywords: Personalised modelling; spiking neural networks; longitudinal MRI data; dementia; classification; prediction.

1. Introduction

The burden of dementia is rapidly rising worldwide [1, 2] with the overall cost increasing from US\$ 279.6 billion in 2000 to US\$ 948 billion in 2016, corresponding to an annual growth rate of 16% [3, 4]. More subtle clinical and cognitive changes take place during a period of mild cognitive impairment (MCI), which is highly prevalent in elderly people (>65 years). However, disparities in the case ascertainment [5] and diagnostic criteria lead to substantial variation in prevalence and incidence estimations of MCI across populations with rates ranging between 10–42% reported [3, 4]. People with MCI are 6–12 times more likely to progress to dementia compared to age-matched cognitively healthy individuals, at a rate of 15–26% during the 1–2 year follow-up and reaching 50–83% during the 3-year follow-up [6, 7]. Approximately 50% of people with MCI spontaneously revert to normal cognitive functioning, but those who revert to no-MCI conditions, still have a greater risk of ultimate transition to dementia [8]. Understanding dynamic brain changes associated with shifts in cognitive function underpinning progression to dementia is critical to addressing the increasing burden of the illness [2], [9]. Considerable judgment is required in making the distinction between healthy ageing people and those with different forms of MCI that would or would not lead to dementia. Although there is neuroimaging evidence for interactions of brain asymmetry in ageing and dementia [10–13], accurate clinical and neuroimaging prediction of cognitively healthy ageing, MCI and dementia is currently limited.

The current paper introduces a novel, personalised predictive method and a computational system for individualised classification and prediction of brain states in a longitudinal neuroimaging ageing cohort. The study contributes to the ‘precision medicine’ concept [14]. The proposed system is built upon a brain-inspired spiking neural network (SNN) architecture and applied for early prediction of cognitively healthy ageing, MCI, and dementia. The relative risk of development from MCI to dementia might be determined based on structural brain data [15–17], including regional brain volume and white matter hyperintensity (WMH), which progressively decline from healthy ageing to MCI and dementia [9], [18–21]. Nevertheless, whilst several biomarkers are associated with reduced cognitive ability and risk of dementia [22–25], substantial discernment is still necessary for distinguishing various potential trajectories of MCI [26] and accurate prediction of clinical outcome remains limited.

Improvement in the accuracy of classification and prediction of cognitive outcomes during human ageing using brain data is warranted and may be possible using advanced machine learning (ML) methods capable of making sense of integrated spatial and temporal components of brain data. Artificial Neural Network (ANNs) are popular ML models that are based on the information processing mechanism of brain *neurons*. ANNs are a set of interconnected computational units representing *neurons*. The networks are computational models that can be trained with input data to generate useful outputs (predictions). Recently, deep learning ANN methods have been effectively applied to a wide range of Magnetic Resonance Imaging (MRI) studies [27], including spatiotemporal denoising of contrast-enhanced MRI [28], [29] artifact detection [30], resolution enhancement [31], and image segmentation [32]. Deep learning Convolutional Neural Networks (CNN) [33] are commonly used for MRI segmentation, such as ischemic lesion segmentation [34] and brain tumour segmentation [35], [36]. Deep learning approaches were also used for MRI feature extraction and identify different stages of Alzheimer’s disease [37], classification of MCI [38], and early diagnosis of Alzheimer’s disease (AD) [39].

Although deep learning techniques are inspired by some properties observed in brain research [40, 41], the mathematical modelling of a perceptron-type ANN computes the outputs with respect to the current time of input vectors. However, activation of a brain *neuron* is influenced by the dynamics of the membrane potential over time. When the membrane potential surpasses a certain capacity, it generates an action potential (signal, spike) that

propagates to other *neurons*. Therefore, the latest generation of ANNs, called Spiking Neural Networks (SNN) [42] can facilitate the development of brain-inspired computational models, in which a *neuron*'s representation resemble the principle of action potential to incorporate previous accumulated inputs and the neurons can evolve their connectivity through learning from data using also learning principles inspired by the brain [43], [44], [45].

SNNs are computational models that consist of spiking *neurons* as processing elements, connections between them, and biologically plausible learning algorithms [46], [47], [48]. Spike Timing Dependent Plasticity (STDP) [49],[50] is a well-known paradigm for learning in SNNs and is the main mechanism for information storage in auto-associative networks [51], [52], [53]. It acts in capturing spatiotemporal patterns of network activity that could efficiently contribute to temporal processing. STDP learning adjusts the neural synaptic weights with respect to the timing of spikes in pre- and postsynaptic *neurons*. Hitherto, STDP has received substantial attention in experimental and computational neuroscience [54],[55],[56],[57]. With STDP, changes in synaptic strength can be modelled to resemble the information processing in nervous systems. Such changes in synaptic strengths are similar to Long-Term Potentiation (LTP) and Long-Term Depression (LTD) [58].

The current paper presents the development of a generic methodology based on brain-template structured SNN architecture and proposes a new personalised predictive system for accurate detection and prediction of cognitive states (healthy, MCI, and dementia) from a longitudinal MRI data. The MRI data were collected in the context of a prospective community-based cohort study, the Sydney Memory and Ageing Study (MAS study), from dementia-free participants at baseline, aged between 70 and 90 years (some of them moved to dementia and MCI states after 6 years). The MRI data were collected at baseline (T1), 2-year follow-up (T2), and 6-year follow-up (T4). The approaches of the MAS cohort study have been previously described elsewhere [59]. Briefly, all participants were assessed in order to diagnose different subtypes of MCI and dementia, normal cognitive functioning or reversion from MCI to normative cognitive condition according to international consensus criteria [8, 59, 60]. Those who met the criteria for dementia at the baseline assessment, were not included in the study.

2. Methods and Materials

This section describes the MRI data that we used in this study as well as the proposed methods for building personalised modelling for prediction of an individual cognitive outcome.

2.1 MRI Data Description

The MRI longitudinal data were collected in the MAS study in Sydney (Australia) [8, 59]. Participants (n=554) without dementia at the baseline, had been recruited into a longitudinal structural MRI study, with data collected at every 3-time points spanning a 6-year period (T1 as a baseline measurement, T2 at the 2-year follow-up, T3 no 4-year follow up, and T4 at the 6-year of follow-up). All participants were assessed at baseline and two follow-ups, in order to diagnose MCI and dementia, normal cognitive functioning or reversion from MCI to no MCI according to international consensus criteria [59, 60]. Participants meeting the international criteria for dementia at the baseline were not included in the study. A subsample of n=175 (mean age = 83, sd= 4.1, 77 males (44%)) were selected because they had data recorded across all assessment points with scores for 31 common MRI features, including WMH and structural volumes (FSL FIRST)¹. Table 1 represents the number of individuals with different cognitive outcomes during the measurement period of the MRI data. It also reports the transition pattern of 14 individuals with dementia (diagnosed at T4) from non-dementia states during the 6-year period of the MAS study. Amongst those 14 participants diagnosed with dementia, only two of them developed dementia from healthy cognitive

¹ FSL FIRST: FSL is a comprehensive library of analysis tools for MRI brain imaging data, and FIRST is a model-based segmentation/registration tool.

condition while others transited MCI state (Table 1-b). The list of MRI features is provided in Supplementary Table 1.

Table 1. (a) The number of individuals with different cognitive outcomes diagnoses (healthy, MCI, and dementia) from T1 to T4. We used 175 MRI samples (each sample relates to a subject) recorded at 3-time points abbreviated by T1, T2, T4 (there was no measurement at time T3). (b) 6-year diagnosis labels across T1, T2, and T4 of 14 individuals who were diagnosed with dementia at T4. Healthy, MCI and dementia labels are respectively denoted by digit codes 0, 1, and 2.

	Diagnosis label	Mean age (Standard deviation (SD) at T1 in years)				T 1	Interval		T 2	Interval		T 3		Interval		T 4
(a)	Healthy	77.0 (4.1)				113	2 years		108	2 years		Not measured		2 years		94
	MCI	78.3 (4.8)				62			64							67
	Dementia	80.3 (4.8)				0			3							14
	Total individuals					175		175				175				
(b)	Six-year diagnosis labels of 14 dementia individuals across T1, T2, and T4															
	Follow ups	1	2	3	4	5	6	7	8	9	10	11	12	13	14	
	T1	0	0	0	1	0	1	1	0	1	0	1	1	1	1	
	T2	2	1	1	2	1	1	1	0	1	1	1	1	1	2	
	T4	2	2	2	2	2	2	2	2	2	2	2	2	2	2	

2.2 MRI Data Measurement and Pre-processing

The scans were acquired using a Philips 3T Achieva Quasar Dual scanner (Philips Medical Systems, Best, the Netherlands) located at the Prince of Wales Medical Research Institute, Sydney, Australia. Acquisition parameters for T1-weighted structural MRI scans were: TR = 6.39 ms, TE = 2.9 ms, flip angle = 8°, matrix size = 256 × 256, FOV = 256 × 256 × 190, and slice thickness = 1 mm with no gap in between, yielding 1 × 1 × 1 mm³ isotropic voxels. FLAIR scans were acquired with TR = 10,000 ms, TE = 110 ms, inversion time (TI) = 2800 ms, matrix size = 512 × 512, slice thickness = 3.5 mm without gap, and in plane resolution = 0.488 × 0.488 mm. Two types of neuroimaging volumetrics were used: (a) subcortical grey matter volumes and (b) WMH volumes. Subcortical volumes were calculated using FreeSurfer (version 5.3.0) [61]. WMH volumes were computed using a fully automated pipeline for extracting WMH [62]. Briefly, individual FLAIR (fluid attenuation inversion recovery) scans were first registered to their corresponding T1-weighted scan. Tissue segmentation was conducted in T1 images to create the warping from individual to Diffeomorphic Anatomical Registration Through Exponentiated Lie (DARTEL) space. The resultant flow maps were applied to warp the FLAIR images in T1 space to DARTEL space. After removing non-brain tissue and bias field from FLAIR images in DARTEL space, FSL's FAST was run to segment FLAIR images into clusters. The clusters were then classified into WMH and non-WMH. The resultant WMH was superimposed to FLAIR images for visual inspection. Periventricular WMH was defined as WMH voxels within 12 mm from a periventricular mask in DARTEL space, and the rest WMH voxels were regarded as deep WMH.

2.3 The Proposed Methodology for Personalised Modelling on Longitudinal Data using SNN, Applied to MRI Data for Prediction of Different Cognitive Outcomes

This section proposes a methodology and a computational framework (shown in Fig. 1), called personalised modelling spiking neural network (PSNN), for predictive modelling on longitudinal data that consists of the following procedures:

1. Selecting nearest neighbouring samples to an individual MRI data.
2. MRI data interpolation.
3. Encoding the temporal sequences of the measured MRI variables into spike trains by:
 - Interpolating the data between points of measurements, so that more data points are generated, forming time series.
 - Encoding the obtained time series into spike trains using spike encoding methods.
4. For each individual i , a PSNN model learns from the input spikes of the neighbouring samples to individual i . The learning algorithm is the unsupervised STDP rule [63].
5. Training an output classifier to learn the relation between the PSNN *connectivity* patterns and the MRI data class labels (healthy, MCI, dementia), and model visualisation.
6. Testing the PSNN classifier on the individual x data.
7. PSNN model parameter optimisation.

The details of the proposed personalised modelling methodology are explained as follows:

2.3.1 Selecting Personalised Nearest Neighbouring Samples

For building a personalised model of an individual x , a group of similar subjects' MRI samples to x at T1 is selected. Then, the longitudinal MRI data (reordered at time points T1 to T4) of these similar subjects are selected as the training dataset. The class label information of these samples is defined with respect to the diagnostic labels at the last measured time point (T4).

The selection of nearest neighbouring samples is performed using WWKNN algorithm [64], where the first W denotes a normalised Euclidean distance between an individual MRI data and other individuals' data at baseline (T1). The second W represents a ranking (weighting) of the MRI features with respect to their discriminative power across samples belonging to different classes. Here, the ranking W is measured by using the Signal-to-Noise Ratio (SNR) method that computes a variable (feature) importance to discriminate samples that belong to different classes. In a C -class problem, where $C = \{1, 2, \dots, n\}$, the SNR value of each feature f is denoted by R_f and computed as follows:

$$R_f = \frac{\sum_{i=1}^n \frac{\text{abs}(\mu_i f - \mu_{\{C \setminus i\} f})}{\sigma_i f + \sigma_{\{C \setminus i\} f}}}{n}, \quad f = 1, \dots, F \quad (1)$$

Here, i indicates one class of samples that is assumed as signal and $\{C \setminus i\}$ refers to the other classes (assumed as noise). The $\mu_i f$ and $\sigma_i f$ refer to the mean-value and standard deviation of a feature f within the samples in class i . The computed R_f is further utilised to modify the distance $D_{x,y}$ between every two individuals' MRI samples x and y as follows:

$$D_{x,y} = \frac{\sqrt{\sum_{f=1}^F R_f (x_f - y_f)^2}}{\sum R_f} \quad (2)$$

Here, F indicates the number of features in data (31), and x_f and y_f refer to the values of f^{th} feature in sample x and y correspondingly. With respect to this computed distance, when an MRI sample x enters to the personalised modelling system, all the other MRI samples are descending sorted with respect to their distances to x . Then, the top k similar samples to x were selected as KNN samples. In our experiments, since the dataset has a small number

of samples in the dementia class (only 14 individuals), we suggested to set a limit to select a maximum number of 14 samples from each group. This ensures that the generated datasets are balanced across the groups. We assigned different values to K , ranging from 5 to 14 and selected different MRI samples for training the SNN models. For all the 175 individuals, $k=14$ resulted in the best accuracy of outcome classification and prediction.

2.3.2 Imputation and Interpolation of Longitudinal Data

We used an imputation technique to deal with missing MRI values. A subset of the most similar subjects to the one which has missing values was selected by KNN algorithm with respect to the Euclidean distance measure. Then the mean value of the distances was imputed to the missing one. Further information about the imputation technique is provided in Section I and Fig 1 of the Supplementary.

To capture the temporal dynamic patterns in the MRI data over the 6-year period, still preserving the trend of changes in the MRI measured data, we simulated one data point per month, plus the data points in T1, T2 and T4, resulting in 75-time points in the 6-year period of data collection in the MAS study. The interpolated temporal patterns were then encoded into sequences of binary events, called spikes, to capture significant upward and downward changes in the MRI time series. Afterwards, we spatially mapped the MRI features into a 3-dimensional reservoir of artificial spiking *neurons*, structured according to a brain template. The SNN model learns the spike encoded spatiotemporal MRI data using a biologically plausible learning algorithm which resembles the information proceeding mechanism in the brain. Using this, the model captures the spatiotemporal interactions between the MRI features over time, resulting in the identification of markers of dementia that are used to predict the cognitive outcomes a few years ahead.

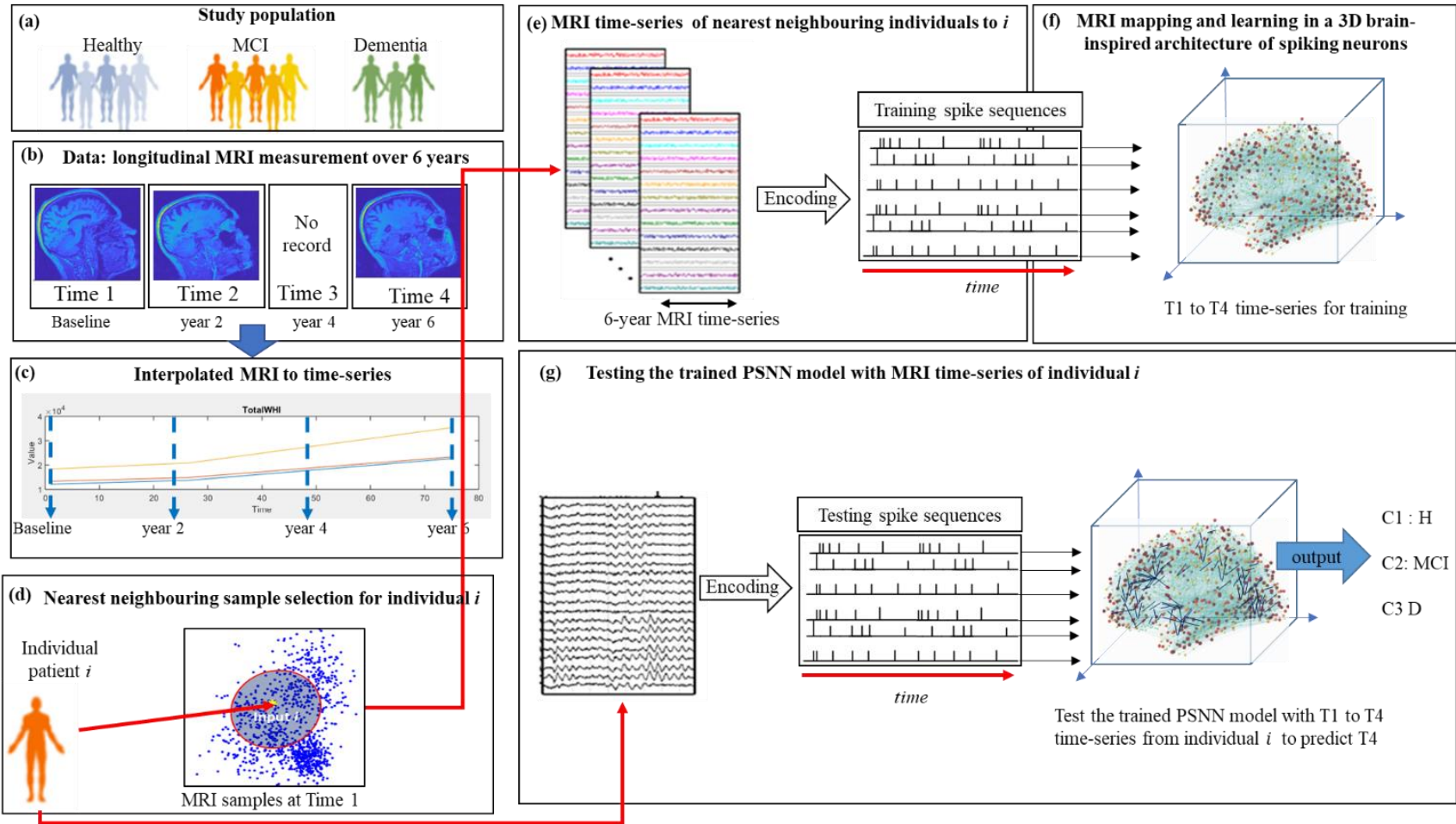
2.3.3 Time Series MRI Encoding to Spikes

Encoding procedure was suggested in several studies for transforming temporal data to certain events in time and provide significant information of dynamic changes in data for computational modelling [65][66][67][68]. In this study, the MRI time series are encoded into spike trains which represent upward or downward changes in the intensity of the MRI features over time. A spike dependant time encoding rule is simulated from neural encoding procedure that relates to the transition of neural signals to electrical pulses, called action potentials. For the encoding method in this research, we employed a threshold-dependant approach to generate spikes which preserve the MRI dynamic changes over time. For a given MRI time series $M(t)$, where $t = 1, 2, \dots, n$, the variation of feature value over time is denoted by $B(t)$, with a baseline $B(1) = M(1)$. At the next time point t , if the feature value is higher than $B(t-1)$ plus a threshold β , then a positive spike is generated at t and $B(t)$ will be replaced by $B(t-1)$. The encoding procedure is defined as follow:

$$spike(t) = \begin{cases} 1 \text{ and } B(t) \leftarrow B(t-1) + \beta & \text{if } M(t) \geq B(t-1) + \beta \\ -1 \text{ and } B(t) \leftarrow B(t-1) - \beta & \text{if } M(t) < B(t-1) - \beta \\ 0 & \text{otherwise} \end{cases} \quad (3)$$

To calculate threshold β , the whole MRI sample length is considered. Here, the threshold β is a self-adaptive bidirectional thresholding method, applied to all features. For an input time series $M(t)$, we calculate the mean m and the standard deviation s of the gradient dM/dt , then the threshold is set to $m + \alpha s$, where α is a parameter controlling the spiking rate (the intensity of the generated spikes) after encoding. In our experiment, we set $\alpha = 0.5$ which resulted in an optimal spike rate for reconstruction of MRI time series from spike trains. The encoding algorithm is provided in Supplementary Table 3, while Supplementary Fig. 2 demonstrates an example of encoding MRI time series to spike trains from Left Thalamus feature across the groups (healthy, MCI and dementia).

232



233

234 Figure 1. A diagram of the suggested generic personalised modelling approach for longitudinal data using SNN illustrated here on the MRI case study data of 6
 235 years for the classification and prediction of individuals cognitive outcomes. (a) the cohort 6-year study includes three groups of individuals (healthy H, MCI
 236 diagnosis, and dementia (D) diagnosis); (b) The MRI data were collected at baseline (T1), 2-year follow-up (T2), and 6-year follow-up (T4); (c) the MRI
 237 measurements were interpolated to time series to capture the patterns of changes over 6 years for each individual; (d) for a new person i entering to the system, a
 238 group of nearest neighbouring individuals to this person is selected using our proposed clustering technique applied to MRI data at T1; (e) the MRI time series of
 239 the nearest neighbouring individuals to i are selected as the training dataset, then transferred to spikes and utilised for training a brain-inspired SNN model; (g) the
 240 SNN model is then tested using the MRI time series (T1 to T4 data) of patient i for classifying this patient to one of the diagnosis labels (H, MCI, D) or tested
 241 using smaller MRI time series (2 years or 4 years) for prediction of outcomes in T4. This procedure is performed for all individuals and the average accuracy is
 242 reported.

2.3.4 Spiking Neural Networks Architecture for Personalised Modelling of MRI

The proposed personalised modelling is built upon SNN architecture. SNNs were introduced for the first time in computational neuroscience for modelling the behaviour of biological *neurons*. Biological *neurons* use action potential (sudden pulses in time) to compute and transmit information. In SNNs the principle of an action potential is computationally replicated by binary events (-1 or 1, called spikes) with precise timing as means of communication. They are biologically plausible neural models comprised of spiking *neurons*, connections between them (synapses), and learning algorithms [46][47][48]. Computational model of a spiking *neuron* allows the *neurons* potential to change as a function of time and input temporal spikes. A spiking *neuron* emits output spike at the time t in which its internal state exceeds a threshold. The generated spikes are propagated over time through the SNN and lead to the adjustment of the *connections*, allowing the model to learn and memorise. A synaptic connection can be an excitation that rises the *neuron's* potential once receiving input, or an inhibitory that reduces the *neuron's* potential [69]. This resembles the biological excitatory and inhibitory neurotransmitters that respectively increase or suppress the postsynaptic *neuron* potential towards firing. Depending on the timing of spikes between a pair of pre- and postsynaptic *neurons*, the connection weights between them can be strengthened or weakened. Therefore, the model learns the causal relationship between the connected *neurons* by adapting the connections. Hence, these SNNs are thought as brain-inspired computational models with biologically plausible properties (action potential, excitatory postsynaptic potential, and inhibitory postsynaptic potential [70]).

The encoded spike sequences of the selected MRI data are transferred into a 3-dimensional model of PSNN which topologically preserves the spatial information of the MRI features. In order to initialise the connections in the PSNN model, the small-world (SW) *connectivity* rule is applied [71][72]. In this rule, every neuron is randomly connected to its nearby neurons within a reduce (fixed to 2 neurons away). The connections are weighted with small random values, so that on average 80% of the them are positive values [0-1] while 20% of them are negative [-1-0] which are normally distributed all over the network [73]. In this study, mapping and initialisation of connections are set the same for all experiments. The mapped PSNN model is then trained by the temporal information of the input spike sequences. When the training procedure with the selected KNN samples of MRI data is completed, the time series of a person x data (excluded from the training) is used to test the model. The trained PSNN model is a personalised model of person x and can be used as an individualised profile to investigate the relationships between a person's MRI features over 6 years in relation to a predicted outcome.

The *neurons* in a PSNN model can be developed according to various computation models including Integrated and Fire model [74], Leaky Integrated and Fire model (LIF) [75, 76], or Izhikevich model [70]. In the current study, we used LIF for modelling the *neurons* in PSNN architecture. In the LIF model after a *neuron* has spiked, its membrane potential will not start increasing with next incoming spikes before a refractory period is over. Between the input spikes, the *neuron's* potential reduces by a leak-parameter (illustrated in Fig. 2).

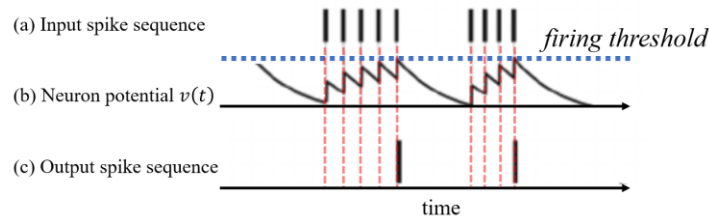


Figure 2. The Leaky Integrated and Fire (LIF) model of *neuron* shows that when an input spike (shown in a) arrives in a *neuron* at time t , the *neuron's* potential voltage $v(t)$ (shown in b) increases towards the firing threshold, while decreases (leaks) between sequential spikes. If the potential reaches a certain threshold (shown by a green horizontal line), then the *neuron* produces an output spike in time t (shown in c) and its potential reset to initial value [77].

2.3.5 Unsupervised Learning in SNN Models with Encoded MRI Spikes

The learning process in this methodology has two phases (unsupervised and supervised learning). Unsupervised learning is for adjusting the initial connection weights (inhibitory and excitatory connections) in the PSNN model while the model is learning from the streaming input MRI spikes. For this learning process, we used the STDP rule [63] which is a biologically plausible unsupervised learning method. The STDP adjusts a synaptic strength regarding the time relation between the presynaptic and postsynaptic action potential occurrences (pre and post spikes) as depicted in Fig. 3.

STDP rule suggests that if two *neurons* have causal relationship, then their connection weight should be increased, and this occurs when the presynaptic *neuron* fires just before the postsynaptic *neuron*. The STDP learning rule is defined using the following relation:

$$\Delta w = \begin{cases} A_+ \exp\left(\frac{\Delta t}{\tau_+}\right) & \text{if } \Delta t \geq 0 \\ -A_- \exp\left(-\frac{\Delta t}{\tau_-}\right) & \text{if } \Delta t < 0 \end{cases} \quad (4)$$

where Δw defines the amount of change in the connection weight between pre and post *neuron* with respect to their spiking time interval $\Delta t = t_{pre} - t_{post}$. The parameters A_+ and A_- define the highest value to modify the connection (when $\Delta t \approx 0$). The parameters τ_+ and τ_- denote the ranges of pre-to-post-synaptic inter spike intervals over which the synaptic strengthening and weakening occurs. Fig. 3 plots the changes in synaptic weight by Δw as a function of postsynaptic spikes in time. STDP allows the SNN models to learn from data with respect to exact timing of spikes, therefore, acting as an efficient learning rule that generates optimal information follow in the networks [49],[78].

2.3.6 Supervised Learning in SNN Models with MRI Data

When the unsupervised learning is accomplished, we performed supervised learning using dynamic evolving SNN (deSNN) [79] method to learn the association between the training MRI samples and the class label information (healthy, MCI, dementia). For every training MRI sample, one *neuron* was created on the output layer and linked to all the *neurons* in the already trained SNN model via excitatory connection. The training samples that were used for unsupervised STDP learning are being passed again to the SNN for supervised training that modifies the output layer connections. In this process, when entering the training samples to the model one by one, the temporal spiking activities in the SNN model, generated by each sample, will be used as input spikes to train the corresponding output *neuron's* connections for recognising this sample. The output connections are first created with weights of zeros and then initialised with respect to the Rank-Order (RO) rule [80]. This rule assigns the highest value to the first arriving spike from a presynaptic *i* in the SNN reservoir a postsynaptic *neuron j* in the output layer when modifying the connection weights $W_{i,j}$ between *neurons i* and *j*. This is defined as follows:

$$W_{i,j} = mod^{order(i,j)} \quad (5)$$

Where mod is a modulation factor within $[0, 1]$ and $order(i, j)$ is the time order (rank) of the arrival of the first spike from the presynaptic *neurons i* to the postsynaptic *j* and the rank is calculated across all presynaptic *neurons* connected to *j*. The range for *i* is from 1 to number of neurons in SNN and the range for *j* is from 1 to the number of training samples as neurons on the deSNN layer.

After the initialisation of the output connections with respect to the first arriving spikes using RO rule, then they will be further modified using a small drift parameter to take into account the occurrence of the following new spikes at postsynaptic *neuron j* at time *t*. When there is no spike to *j* at time *t*, then the corresponding connection weight decreases by the drift parameter, otherwise, it increases. After applying the deSNN supervised learning

phase, the output connection weights are fixed. Next, in the validation phase, a new MRI sample, which is unknown to the model, is used for testing. For this sample, an output testing *neuron* is generated and connected to the *neurons* from the SNN reservoir. Then, these output connections will be adjusted while propagating the spike trains of this MRI sample to the model. When the output connections are established, this *neuron* will be classified by KNN algorithm that computes the distance between this newly formed testing *neuron* connections and the rest of the output *neurons* connections. The algorithm then votes on a class label of which the new output *neuron* is similar to the majority of the output *neurons* in the KNN set labelled with the same class. This process is performed for all the testing samples by building different personalised SNN models for testing the outputs for the samples and for classifying them.

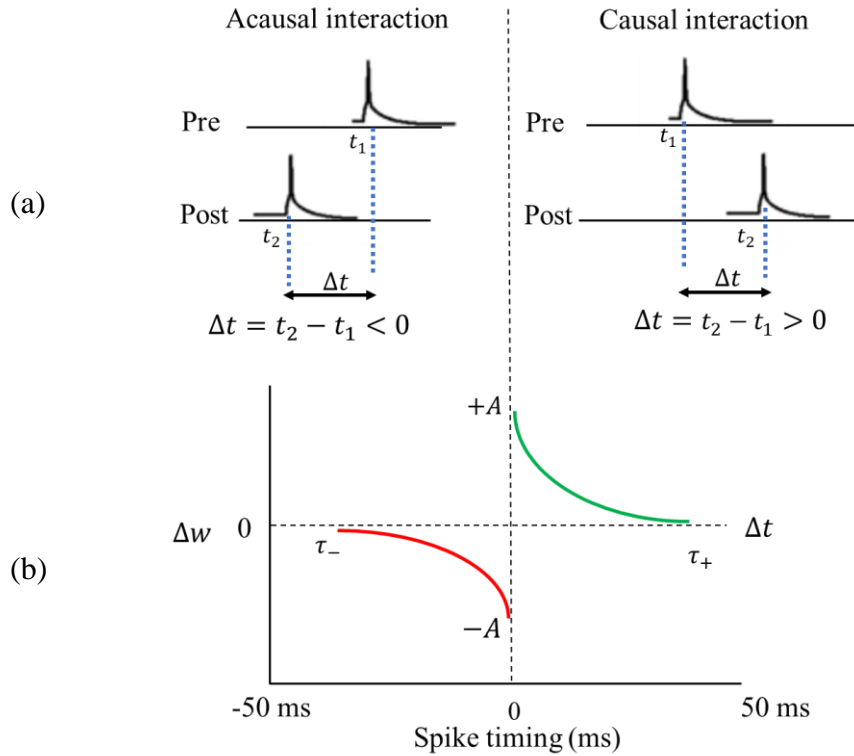


Figure 3. STDP rule adjusts the synaptic weight by Δw value depending on the time relation between the presynaptic and postsynaptic spikes occurrence. (a) If presynaptic *neuron* (Pre) fires at time t_1 just before the postsynaptic neuron (Post) fires at t_2 , then $\Delta t = t_2 - t_1 > 0$ indicates a causal relationship that leads to increase the synaptic weight by a positive Δw value if the Post spike is within τ_+ time interval. On the other hand, $\Delta t < 0$ leads to decrease the synaptic weight by $-\Delta w$ value; (b) the changes of synaptic weight Δw as a function postsynaptic spikes in time. The spike of presynaptic or postsynaptic *neurons* are denoted by the shorthand notations Pre and Post.

2.3.7 SNN Models Parameter Optimisation

The SNN models' parameters are optimised using a grid-search technique to reduce the classification and prediction outcome error. The optimised parameters are: SNN learning rate and the classifier parameters (mod and drift). In grid-search technique, each selected parameter was searched within a range specified by the minimum and maximum value (SNN learning rate (interval [0.001-0.03]), modulation factor mod (interval [0.4-0.95]) and drift (interval [0.001-0.3]), through several iterations related to the number of steps for moving from minimum to maximum. We assigned 10 steps between the minimum and maximum values of each parameter range. Therefore, for every individual i , 1000 iterations of training (using all MRI samples except the holdout sample i) and testing (using the single holdout sample i) were performed with a different combination of these three parameters. For

every PSNN model, the parameter values that resulted in the best accuracy in most of these 1000 iterations, were selected as the optimal parameters.

The proposed methodology here is based on SNNs as powerful models for modelling complex spatiotemporal data due to their speed, efficiency, real-time action, and biological fidelity [81],[42],[82]. In this study, we used computational SNN models with biologically plausible STDP learning algorithm for mapping, learning, visualising, classification, and prediction of cognitive outcomes (healthy, MCI, dementia) using longitudinal MRI data. The learning process included both unsupervised (STDP rule) and supervised learning (deSNN algorithm). The hyperparameters of the models were optimised using a grid-search approach. The SNN models with STDP learning transpired as a potential means to understand time, space, and frequency of complex spatiotemporal brain data. The main advantages of using brain-inspired SNN models is to reveal patterns of spatiotemporal interactions of input variables to suggest possible markers of dementia-related diseases. (3) There are powerful neuromorphic hardware systems of thousands and millions of *neurons* working in parallel, that can speed up the computation in a real-time for real-world applications. An example is SpiNNaker which is used in the neuromorphic platform for the Human Brain Project [83],[84]. (4) Predictive modelling of spatiotemporal brain data using SNNs and their biologically plausible spike-dependant learning algorithms has shown greater prediction accuracy than traditional ML methods.

3. Results

Fig. 4 illustrates the main phases of the proposed methodology applied to the longitudinal MRI brain data. It can be seen that the MRI data of MAS cohort were mapped into a 3D brain-template SNN model that topologically preserves the spatial information of the brain regions while learning from the MRI dynamic changes over time. The spatial mapping in SNN model is based on the Talairach brain atlas [85], which is one of the most frequently employed systems for exhibiting coordinates in neuroimaging studies and was implemented in both BrainMap [86] and Talairach Daemon [87]. The current study used the 3D anatomical Talairach atlas coordinates (x, y, z) with 1471 *neurons* defined according to the stereotactic system and MRI-Electroencephalogram sensors [88] with every computational *neuron* mapping approximately 1-mm³ area of the brain. The applied Talairach template includes anatomical regions classified by lobe, hemisphere, tissue (i.e. grey/white matter) and Brodmann areas [89]. Using this spatial information, the MRI features were mapped into input *neurons* of a Talairach structured 3D SNN with respect to their corresponding anatomical positions (regions of interest in the brain) associated with Talairach regions. Then, the SNN model was trained using MRI time series (input data) to capture spatiotemporal interactions between MRI features over time related to individualised outcomes. Therefore, the spiking activities of a certain cluster of *neurons* can be associated with the activities of a corresponding anatomical region in the human brain.

The trained brain-inspired SNN models capture the spatiotemporal relationships in the data for the detection and prediction of cognitive states (healthy, MCI, dementia). The pipeline procedure includes the following steps:

1. MRI data interpolation to time series. This is to capture the trend of changes in MRI across different individuals in the 6-year period.
2. Personalised modelling for classification of individual cognitive outcome using MRI data across 6-years, for potential marker discovery of MRI changes and a better understanding of the brain dynamics related to the progression of MCI and dementia.
3. Personalised modelling for early prediction (2 and 4 years earlier) of individual cognitive outcome by building a model on full data and testing it on the first 4-year and first 2-year personal MRI data respectively.
4. Visualisation of the personalised models built on MRI data for visual exploration and explanation purposes.

5. Personalised profiling of an individual model for the purpose of finding potential markers for this individual or groups of individuals.

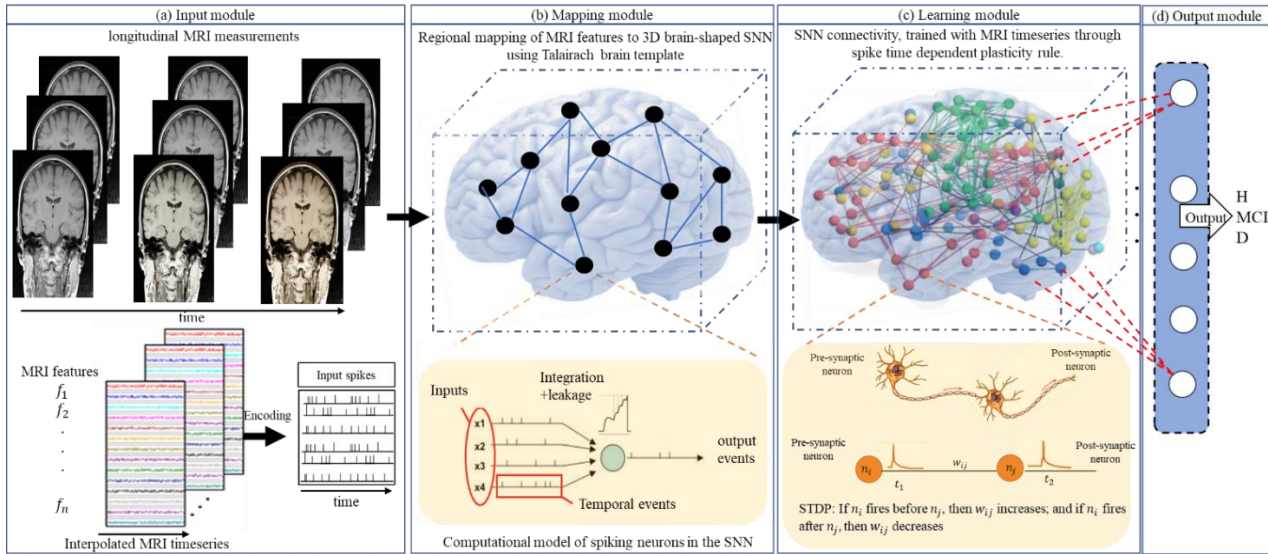


Figure 4. The methodology for modelling of longitudinal neuroimaging data in a 3D brain-template structured SNN architecture, with biologically plausible neurons and learning algorithms. (a) input module consists of method for interpolating neuroimaging data, recorded from several MRI features f , to time series which are then encoded to spike trains and used as input steams to the SNN model; (b) spatial mapping of the SNN model using anatomical locations of the brain areas defined in Talairach space [88] and assigning the input MRI features to input neurons with respect to their Talairach brain regions. Here, the computational model of a neuron is the Leaky Integrated and Fire (LIF) model, where the neuron's potential increases or decreases (integration and leakage) with respect to the incoming events (spikes) in time (see Methods section for details). (c) the mapped SNN model learns from the input spikes to adapt neural connectivity with respect to temporal relationship between pre- and postsynaptic action potentials (spikes between the connected neurons). This is performed by a biologically plausible learning rule (unsupervised spike timing dependant plasticity rule, explained in the Methods section). (d) the output module is based on supervised learning to learn the association between the class labels and the training MRI samples (output neurons). Then the trained model is tested using a new unseen MRI sample for classification of the generated spatiotemporal patterns in SNN into different classes, in this case healthy (H), mild cognitive impairment (MCI) and dementia (D).

3.1 Longitudinal MRI Data Interpolation to Time Series

The original MRI datasets were recorded at baseline, 2-years, and 6-years of follow-up, in the form of static neuroimaging data. To learn the changes in longitudinal MRI data as a function of time in an SNN model, the data from each individual were linearly interpolated to time series by adding simulated data points that illustrate stepwise changes between every 2-time points, from T1 to T4. Here, 24-time points were interpolated for every two-year period, representing one data point per month (in total 72 data points were generated from each subject's MRI longitudinal data series). The obtained time points for the longitudinal MRI data of an individual represent time series information which is used in this paper to create brain-inspired SNN models for predictive data modelling of cognitive outcomes. This interpolation is to transform the static MRI data (measured at 3 points) into time series. The applied linear interpolation is based on a simple assumption to generate more data points between the original MRI measurements while preserving the trend of data. There is no loss of trend-information in this method as the interpolated data points follow the trend of changes in the original MRI data. These changes are then encoded into events in time that capture the dynamics of data changes over time, and then the temporal events are used as inputs for training computational models. The longitudinal MRI data points represent changes in the values from several brain regions of interests (ROIs) over time. We identified 31 MRI variables which were measured as mutual

variables at all the follow-up assessments (T1 to T4). Please see the list of 31 MRI variables in Supplementary Table 1.

Fig. 5 shows an exemplary MRI feature (right pallidum) interpolated to time series. The three temporal patterns of pallidum MRI feature represent the mean value of the feature across all the individuals in healthy (blue line), MCI (red line) and dementia (yellow line) groups based on the diagnosis/outcome provided at time T4. The interpolation of all the MRI features to time series is shown in Fig. 1 of the Supplementary.

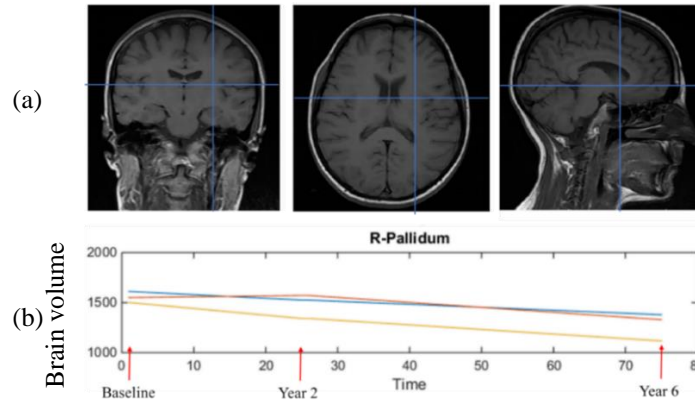


Figure 5. (a) Demonstration of the right Pallidum region in the brain from different angles. (b) The interpolated data representing the trends of changes in the brain volume of one MRI feature (right Pallidum- please see Table 1 in the Supplementary Material) for 6 years, averaged across individuals in healthy H (blue), MCI (orange) and dementia (yellow) outcome groups.

To analyse the MRI changes from T1 to T4 across the groups (healthy, MCI and dementia), Analysis of Variance (ANOVA) [90] was applied to measure the significant distinctions between the groups. A repeated-measures ANOVA was applied with respect to three within-subjects' factors: *Hemisphere* (left and right), *Site* (15 brain sites) and *Time* (T1, T2 and T4) across all the *Groups*. The results (shown in Supplementary Tables 2) suggest a significant main effect of *Time* [$F(14, 258.5) = 309.8, p < 0.001, \eta^2 = 0.64$], two significant *Site*Time* interactions [$F(28, 567.8) = 117.70, p < 0.01, \eta^2 = 0.41$], and a *Site*Group* interaction [$F(28, 258.52) = 2.74, p = 0.04, \eta^2 = 0.03$]. It can be seen from Supplementary Table 2 that at T1, the *Site*Group* interaction did not significantly differ at all brain sites except frontal, anterior horn, periventricular, occipital, posterior horn, and hippocampus. However, the ANOVA analysis showed significant group differences at T2 [$F(28, 258.5) = 1.89, p = 0.03, \eta^2 = 0.21$]. Note that WMH volume reflects lesioning in the white matter. The subcortical volumes are structural volumes, with higher volumes suggesting less atrophy. Compared to healthy and MCI groups, the dementia group showed significant neural changes of WMH volumes in frontal, anterior horn regions, and volumes of the periventricular, occipital, posterior horn, hippocampus, putamen, pallidum, and amygdala. At T4, the *Site*Group* interactions differ significantly at all the brain sites [$F(28, 258.64) = 4.09, p < 0.001, \eta^2 = 0.45$]. Fig. 6 illustrates the change in mean values of MRI features as a function of *Groups*. Sites 3 (frontal) and 8 (parietal) diverge considerably between MCI and dementia groups and may, therefore, be potential markers for predicting dementia. A significant change from time T1 to T4 is seen in dementia more than MCI. The ML and computational models were used to achieve a deeper analysis of the patterns of MRI changes (within and between the groups), to improve the model and understand these changes. The following presents the creation of a computational model based on deep brain-inspired SNN for personalised modelling of data and to perform pattern recognition, classification, and prediction of cognitive outcomes.

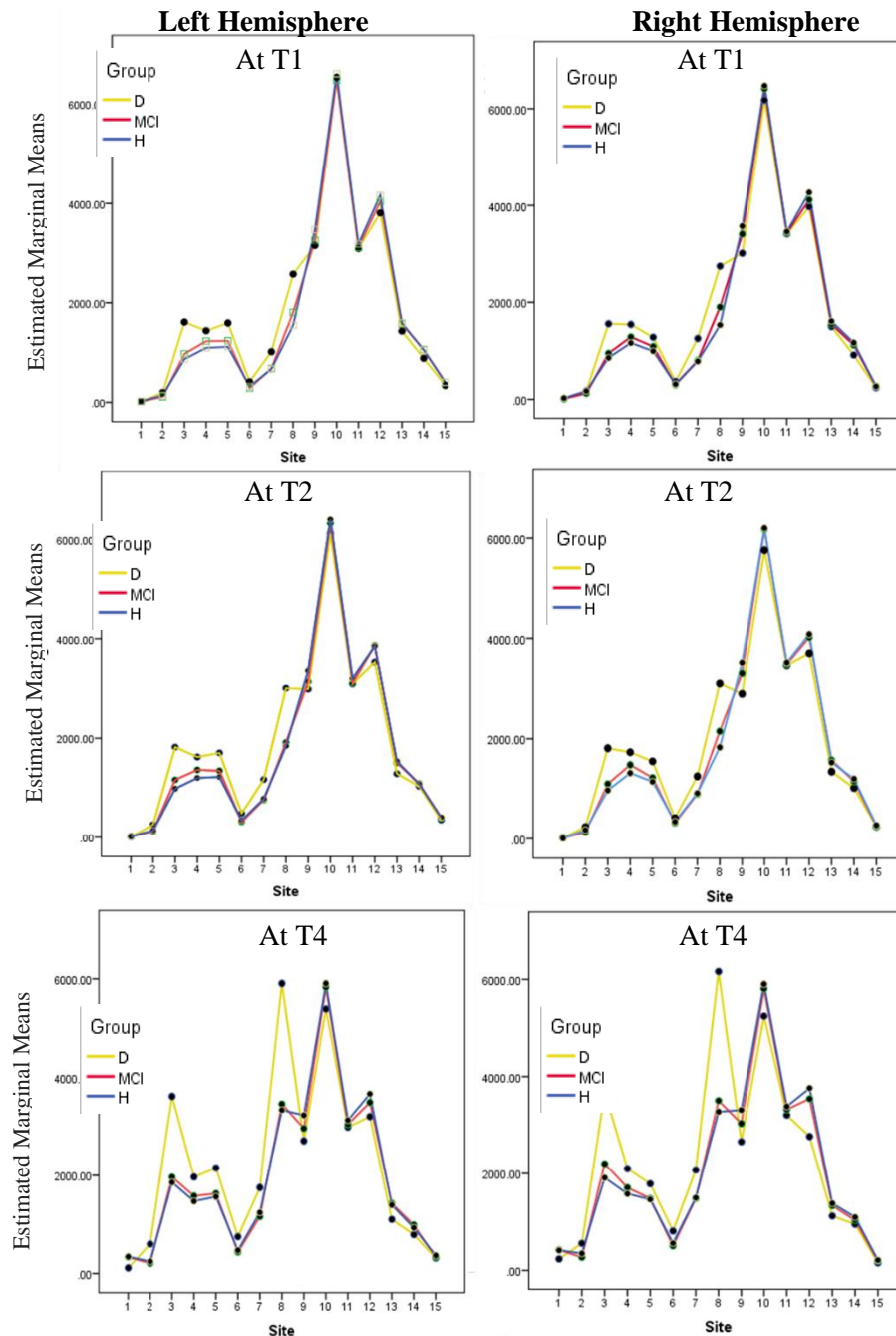


Figure 6. Illustration of the mean values (in mm^3) of the MRI features at 15 brain sites for each of the three subject groups (healthy H, MCI, and dementia D) across the left and the right hemispheres at times T1, T2 and T4 of the MAS study. The brain sites are: (1) cerebellum, (2) temporal, (3) frontal, (4) anterior horn, (5) periventricular, (6) occipital, (7) posterior horn, (8) parietal, (9) Hippocampus, (10) Thalamus, (11) Caudate, (12) Putamen, (13) Pallidum, (14) Amygdala, (15) Accumbens. Features (1)–(8) are WMH volumes and (9)–(15) are Brain volumes FSL (please see Supplementary Table 1 - List of MRI features used in this study). Significant changes from time T1 to T4 are seen in dementia more than MCI and H. Analysis of variance is reported in Supplementary Table 2.

3.2 Personalised Classification of Individual's Cognitive Outcome (Healthy, MCI, or Dementia) using 6-year Interpolated MRI Data

After interpolating the MRI data as time series (Supplementary Fig. 1), personalised classification of healthy, MCI and dementia outcomes (called classes) was performed using computational models for every individual as reported in Table 2. Here, the class label of each individual's MRI data is given with respect to the individual's cognitive outcome diagnosed in year 6 (T4) of the MAS study. For every person i , a personalised SNN model (PSNN) was created and trained by 6-year MRI data (time series from T1 to T4) that belong to a group of similar individuals to person i (similar MRI samples) and this person's data is used only to test the accuracy of the output produced by the model.

Since dementia class (minority class) has a very small number of samples (14), we limited the number of nearest neighbouring samples to 14 which represents selecting a maximum number of top 14 similar samples to i from each of the three classes. This led to select 42 KNN (K-nearest neighbour) samples when creating a model for each individual from H and MCI groups (14 samples per class). In the dementia group of 14 individuals, there were 41 KNN samples for each individual's model (14 from H, 14 from MCI, and 13 from dementia).

The selected KNN samples are used as the training dataset, while the one MRI sample (spatiotemporal sequence) of person i was used as the testing sample, which was excluded from the training phase. The PSNN model of person i was trained using all the KNN samples (sequences) in two phases: unsupervised and supervised learning. The unsupervised learning was based on a spike timing dependant learning rule (STDP) specified for SNN architecture (see Methods section). This learning phase adjusts the spatiotemporal connections in the PSNN model while learning from the input spikes of the training samples. The supervised learning was performed to learn the association between the class labels and the 3D SNN models created for the same training samples. Then the trained model was tested using the 6-year MRI data of the person i who was excluded from the training phases, to classify this person's data into H, MCI or D. This procedure was performed for every individual in the dataset, providing an individual (personalised) classification model. Table 2 reports a high classification accuracy of 96% with respect to individuals' diagnostic outcomes at year 6. This suggests that the personalised models were successfully trained with 6-year MRI time series and captured discriminative patterns of MRI changes for each individual across the groups, and also models to be potentially used for predictive modelling as explained in Section 2.3. The SNN models' parameters are optimised using a grid-search technique to reduce the classification and prediction outcome error. More information about the optimisation procedure is provided in the Methods and Supplementary sections.

Table 2. Personalised modelling for classification of interpolated MRI data to class 1: healthy; class 2: MCI and class 3: dementia subjects using the proposed PSNN method on the MAS study data. The best accuracy for each individual's model was obtained with respect to a grid-search optimisation approach to tune a combination of some PSNN parameters without using the individual's data in the training set (see the Methods section). The reported parameters are the average optimal values across all the 175 individuals' models (Supplementary Figs. 3,4,5). In every personalised model of H and MCI individuals the size of KNN is 42, while KNN is 41 for individuals from dementia group. The table's diagonal represents the number of correctly-classified MRI samples.

Predict \ Real	H	MCI	D	Accuracy	Sensitivity	Specificity	Total accuracy	F-score
Healthy	91	0	0	97%	100%	96%	95%	94%
MCI	3	65	1	97%	97%	97%		
Dementia	0	2	13	93%	98%	92%		
sum	94	67	14					

3.3 Personalised Prediction of Individual Cognitive Outcome

To investigate how early the discriminative patterns of changes in MRI data between healthy, MCI and dementia groups can be captured for prediction of individual outcomes, we performed two personalised predictive modelling experiments. The first experiment was related to the prediction of cognitive outcomes 2 years ahead of an actual diagnosis/outcome. Here, for each individual x , a PSNN model was trained using MRI data from T1 to T4 (6-year data) of the nearest neighbouring individuals to x (selected at T1). Then the model was tested with MRI data from T1 to the generated T3 from the interpolated data MRI values (4-year data) that belong to individual x as reported in Table 3, which constitutes 2-year ahead prediction of an outcome. The second experiment was related to 4-year ahead prediction. Here, for each individual x , a PSNN model was trained using the same training data in experiment 1, but was tested using the MRI data of the individual x from T1 to T2 (2-year data), which results in a 4-year ahead prediction of an outcome for x , as shown in Table 4.

As previously mentioned, for these two experiments the testing MRI data were not included in the training phase when creating a personalised modelling of individual x .

Table 3. Two-year ahead prediction accuracy of MRI data to class 1: healthy; class 2: MCI and class 3: dementia subjects using the proposed PSNN method on the MAS study data. The best accuracy for each individual's model was obtained with respect to a grid-search optimisation approach to tune a combination of some PSNN parameters (see the Methods section). The reported parameters are the average optimal values across all the 175 individuals' models. The table's diagonal represents the number of correctly-classified MRI samples. In every personalised model of H and MCI individuals the size of KNN is 42, while KNN is 41 for individuals from dementia group. The PSNN models are trained by T1 to T4 MRI data (6 years data) and tested using the first 4 years data (equal to 48-time points).

Predict \ Real	H	MCI	D	Accuracy	Sensitivity	Specificity	Total accuracy	F-score
Healthy	88	2	0	94%	93%	97%	91%	89%
MCI	4	63	2	94%	94%	94%		
Dementia	2	2	12	86%	86%	97%		
Sum	94	67	14					

Table 4. Four-year ahead prediction accuracy of MRI data to class 1: healthy; class 2: MCI and class 3: dementia subjects using the proposed PSNN method on the MAS study data. The best accuracy for each individual's model was obtained with respect to a grid-search optimisation approach to tune a combination of some PSNN parameters (see the Methods section). The reported parameters are the average optimal values across all the 175 individuals' model. The table's diagonal represents the number of correctly-classified MRI samples. In every personalised model of H and MCI individuals the size of KNN is 42, while KNN is 41 for individuals from dementia group. The PSNN models are trained by T1 to T4 MRI data (6 years of data) and tested using the first 2 years of data (T1 to T2 equal to 24-time points).

Predict \ Real	H	MCI	D	Accuracy	Sensitivity	Specificity	Total accuracy	F-score
Healthy	73	11	1	78%	82%	78%	73%	67%
MCI	15	46	3	69%	82%	68%		
Dementia	6	10	10	71%	88%	76%		
Sum	94	67	14					

Table 5 shows the results when using LSTM (long short-term memory) which is an artificial recurrent neural network architecture for classification and prediction of MRI data to class 1: H; class 2: MCI and class 3: dementia.

Table 5 Classification and prediction of interpolated MRI data to H, MCI and dementia groups. For classification tasks, MLR (Multiple Linear Regression) and LSTM (long short-term memory) were applied. The prediction was performed only using LSTM in which the model handles different lengths of samples for testing data. The model exactness was measured using F-Score, specificity, and sensitivity. The method is Leave-one-out cross validation.

	Accuracy	Specificity	Sensitivity	F-Score	Parameters
Classification using MLR	73%	%80	%65	70%	NA
Classification using LSTM	43%	69%	58%	56%	BiLSTM. 100 hidden units. layers: 3. Softmax.
2-year Prediction	40%	60%	45%	40%	
4-year Prediction	41%	66%	56%	46%	

Supplementary Fig. 4 reports the optimal STDP, mod and drift parameters in 175 individuals' models. In Table 6, we reported the average of the optimal parameters across all the 175 generated PSNN models. The rest of the parameters are fixed according to previous studies (spike rate parameter= 0.5, small-world *connectivity* radius= 2.5, and *neuron* firing threshold= 0.5).

Table 6. Optimised parameters in the SNN models for classification and prediction of cognitive outcomes (healthy, MCI, dementia). The best accuracy for each individual's model was obtained with respect to a grid-search optimisation approach to tune a combination of some PSNN parameters including SNN learning rate (interval [0.001-0.03]), modulation factor mod (interval [0.4-0.95]), and drift (interval [0.001-0.3]). The reported parameters are the average optimal values across all the 175 individuals' models (Supplementary Figs. 3—5).

SNN models	learning rate	mod	drift
Classification	0.02	0.5	0.22
2-year ahead prediction	0.02	0.5	0.22
4-year ahead prediction	0.01	0.4	0.25

The optimised parameters were validated using a new dataset of 90 samples, generated using Synthetic Minority Over-Sampling Technique (SMOTE) [91] as an up-sampling technique to generate new samples (artificial data) based on the similarities between the feature spaces in the existing dataset. The classification, 2-year, and 4-year ahead prediction results are reported in Supplementary Table. 4.

3.4 Visualisation of the SNN Models

The interpolated MRI time series are first transferred into spikes that represent the changes in the values of brain data features over time. The spike sequences of the MRI features were then mapped into the 3-dimensional SNN reservoir, constructed with 1471 artificial *neurons* using the brain Talairach coordinates [85], enabling the topological preservation of the spatial MRI information. For every MRI feature there is one *neuron* (input *neuron*) allocated in the SNN model to transfer the MRI spike sequences for incremental learning. The SNN connections are initialised with respect to the small-world (SW) *connectivity* rule [71],[72], [92]. The SW rule is a biologically inspired technique which defines the possibility of connecting one *neuron* to other ones with respect to the pairwise distance between them, a greater distance leads to a smaller probability of *connectivity*. To ignore the effect of random initialisation across the groups, we used the same initialised SNN model in all experiments. These initial connections are later modified while the SNN model is learning from the streaming MRI spikes entered through the input *neurons*. The developed SNN model generates a *connectivity* structure, where many-to-many *neurons* are

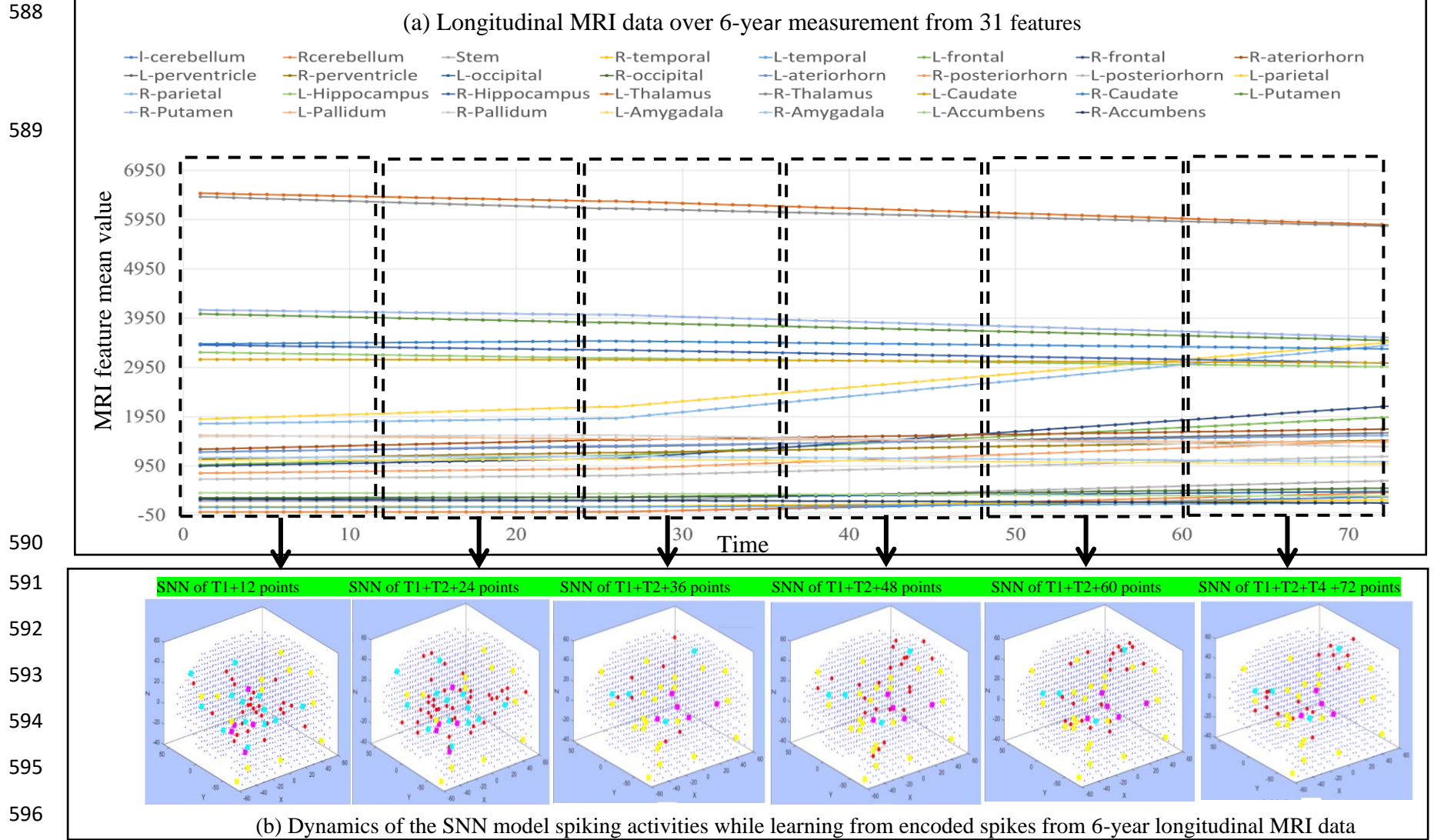
linked to demonstrate the dynamics of longitudinal MRI data. To demonstrate how the spiking activity is propagated into the SNN model while streaming input time series, Fig. 7 shows a stepwise visualisation of spiking activities during the learning process with input MRI data from the MCI group.

Fig. 8 illustrates the modified connections in three SNN models trained separately by all MRI samples (all individuals) from healthy, MCI and dementia groups (diagnoses were taken from T4). This shows that a greater amount and stronger connections were generated in the SNN models of dementia with an average connection weight of 1.1 as compared with the SNN models of MCI (connection weight = 0.93) and H (connection weight = 0.87). These connections were established differently between the groups because of the variation in spike intensities in their longitudinal MRI datasets.

To show how each MRI feature has developed different *connectivity* inside the SNN models of healthy, MCI and dementia groups, we extracted the models' quantitative information and illustrated the average connection weights around each MRI feature in the SNN models (Fig. 9). It can be seen from Fig. 8(c) and Fig. 9 that the SNN model of dementia shows greater spatiotemporal *connectivity* compared to the other groups. This suggests that compared to H and MCI, the dementia group showed greater change across several brain areas, leading to the generation of more spikes. When these spike trains are entered to the SNN model for the learning phase, they result in developing stronger spatiotemporal connections between the model's *neurons*.

For the learning algorithm in the SNN models, we used STDP [63] which can capture the dynamic patterns of MRI data. During the STDP learning process, input spikes are propagated to the model and lead to the adaptation of the spatiotemporal *connectivity*. From Figs. 6 and 9, it can be derived that over the 6-year follow-up in the MAS cohort, several brain regions underwent change in the subjects with dementia diagnoses compared to MCI and H groups. More specifically, these changes were in the temporal, frontal, cerebellum, occipital, parietal, and brain stem sub-areas. This finding can be further studied as neuroimaging predictive markers.

As mentioned earlier, the mapped SNN models in Figs. 8 and 9 were generated when all the subjects' data were used as the training set to capture between-group differences. The next section represents that the proposed personalised modelling allows the creation of an individualised model for each subject's MRI data that is trained with the most relevant individuals' MRI data (nearest neighbouring samples), thus, detecting within-group differences through creating personalised profile for everyone.



597 Figure 7. (a) The mean values of the interpolated MRI time series from 31 features measured over 6 years. MRI features are WMH volumes and brain volumes
 598 FSL (Supplementary Table 1). (b) Six sequential states of spiking activities in an SNN model during STDP learning with 6-year MRI data. The spiking activities
 599 generated during the learning process are visualised after learning from every 12-month MRI data, reflecting the dynamics of MRI features and the corresponding
 600 activated brain areas. Red dots are active *neurons* that just generated output spikes; blue dots are inactive *neurons* that have not yet emitted output spikes; pink,
 601 blue, and yellow squares represent respectively the positive, negative, and no spikes entered from the input *neurons* (MRI features).

3.4. Personalised Profiling of an Individual

The proposed PSNN model can be also used here to derive a personal profile of an individual's cognitive progression over time that can be further investigated in terms of important individual characteristics and risk factors. This personalised modelling approach contributes as a decision support system that allows, for the first time, to create a personalised profile of a person and demonstrates the interactions between the MRI features. Therefore, it supports the model interpretability, which means that we can understand how the MRI feature interactions led to predict a specific individual cognitive outcome (in this case: healthy, MCI or dementia) over 6 years. This is in contrast with many conventional classifiers, which perform like black-box information processing systems[93] with no supporting information to interpret the outcome results. Fig.10 illustrates PSNN models for three randomly selected individuals from H, MCI, and dementia groups. These PSNN models are generated after the unsupervised learning with input spike sequences from different KNN samples of MRI data.

To further analyse the spatiotemporal interactions between the MRI features in the PSNN models of Fig. 11, a Feature Interaction Network (FIN) is created to represent the level of interactions and to measure how the changes in one brain area can be influenced by the changes in other areas. To compute the level of interaction between the input *neurons* (MRI features) in the SNN models, an affinity $N \times N$ matrix A is defined on the SNN model that displays the sum of the spikes that are exchanged between *neurons* i and j ($i = 1, \dots, N$ and $j = 1, \dots, N$) via connection w_{ij} . Every input *neuron* forms a cluster of *neurons* around itself that received the greatest number of spikes from this input neuron compared to the other input *neurons*. The FIN depicts how these groups of *neurons*, each connected to an input *neuron* (MRI feature) are interacting over time. The amount of spike interaction between any two adjacent groups of *neurons* (each connected to one input *neuron*) was computed with respect to the number of spikes exchanged between them. The wider the arc between nodes, the more spikes were transmitted between the corresponding groups of *neurons*, that represent different areas of the brain data model.

In Fig. 11, the FINs show the causal relationship between the 31 MRI features during the learning process in the PSNN models with 6-year MRI data of different individuals' data. The nodes represent the MRI features, while the arcs capture the number of spike communications between the neural clusters around the features during the learning. The thickness of the arcs corresponds to the strength of the interactions between the MRI features. This is observed in Fig. 11 that various interactions between the MRI features were captured for each of the groups. This means that the changes in one MRI feature caused some changes in other ones. The FINs demonstrate that compared to the H group, causal interactions are stronger in MCI and much stronger in the dementia group. For example, in the FIN of MCI, a few noticeable interactions are related to the causality between regions of occipital, accumbens, and periventricular. Also, there is evidence of an association between MRI features in the basal ganglia (right caudate and right accumbens). A strong interaction can also be seen between the amygdala and per ventricle changes; and between right anterior horn and right caudate. The FIN of dementia represents greater brain changes were captured between wider areas of the brain during the 6 years of follow-up compared to healthy and MCI groups. The strong interactions are among left and right anterior horn; left anterior horn and left caudate; right posterior horn and right amygdala; right parietal and right frontal; right occipital and right caudate. The connections have shown causal changes to the cerebellum (posterior), accumbens (subcortical) and frontal cortex (anterior).

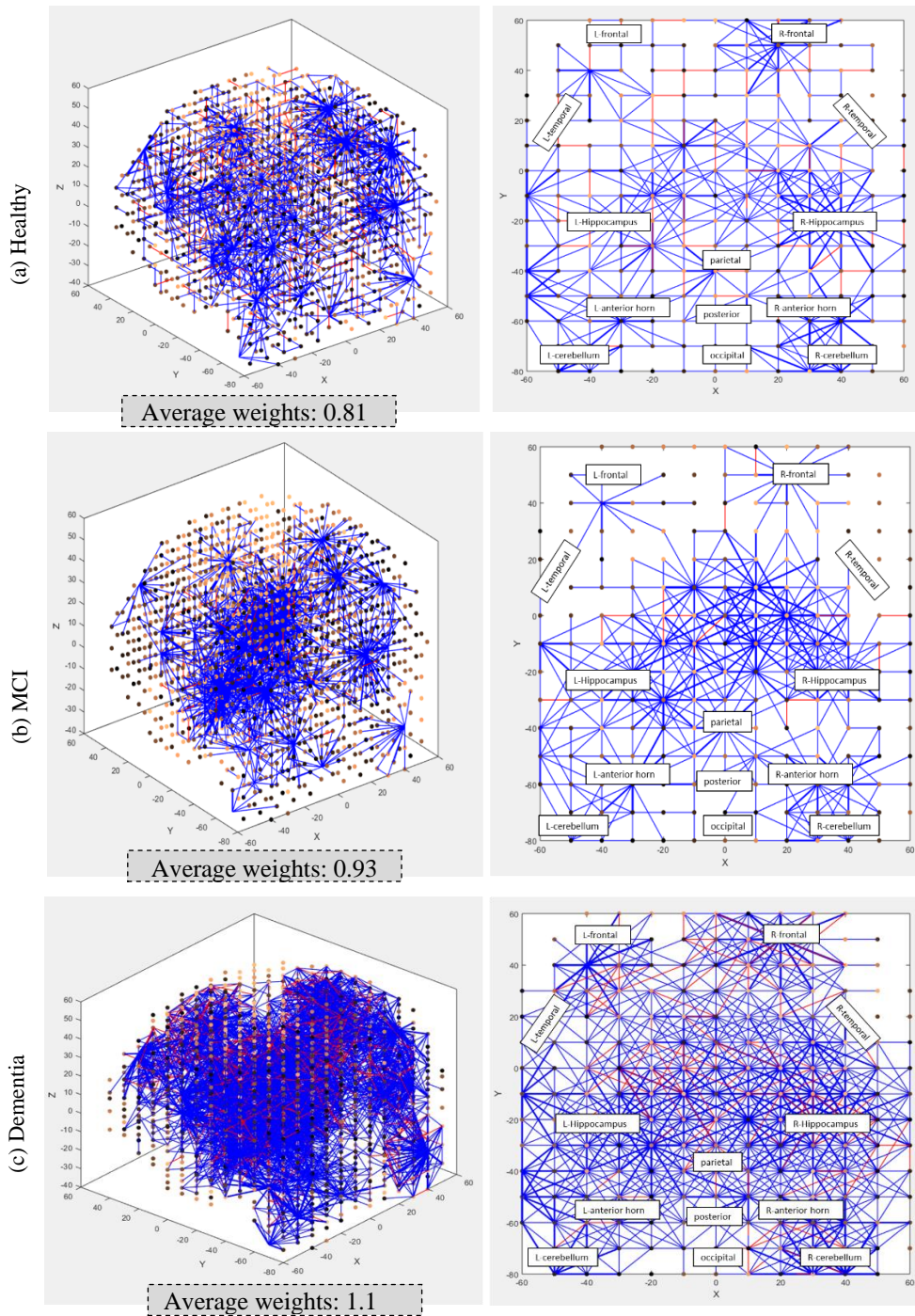


Figure 8. 3D (left) and 2D (right) visualisations of the spatiotemporal *connectivity* in the SNN models trained on MRI data (interpolated from T1 to T4) of individuals whose diagnostic outcomes at T4 are healthy (94 subjects, shown in a), MCI (67 subjects, shown in b) and dementia (14 subjects, shown in c). The SNN model of the dementia group (in c) illustrates greater connections (average weights= 1.1) when comparing with the models of H (average weights= 0.93) and MCI (average weights= 0.81). This is because the values of some of the MRI features have been significantly changed over the 6-year follow-up in MAS study, resulting in enhanced connections between the *neurons* during the SNN model's learning phase. The blue lines are positive (excitatory) connections, while the red lines are negative (inhibitory) connections. The thickness of the lines identifies the weight of the connections.

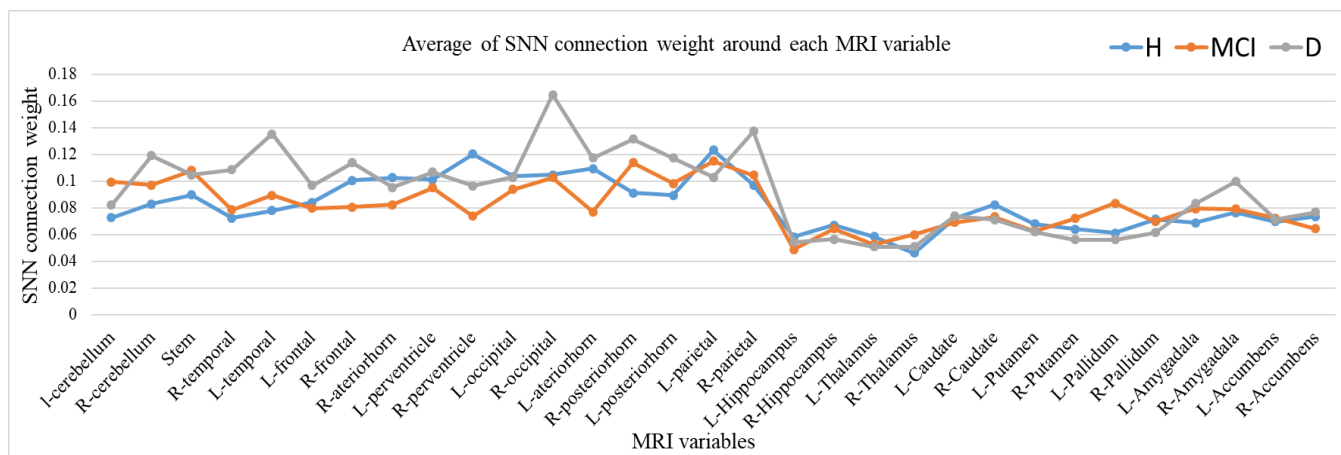


Figure 9. Average connection weights around each MRI variable in the SNN models trained with 6-year MRI time series from healthy H (in blue), MCI in (orange), and dementia D (in grey). Connection weights in the SNN model capture spatio-temporal changes in the MRI input features.

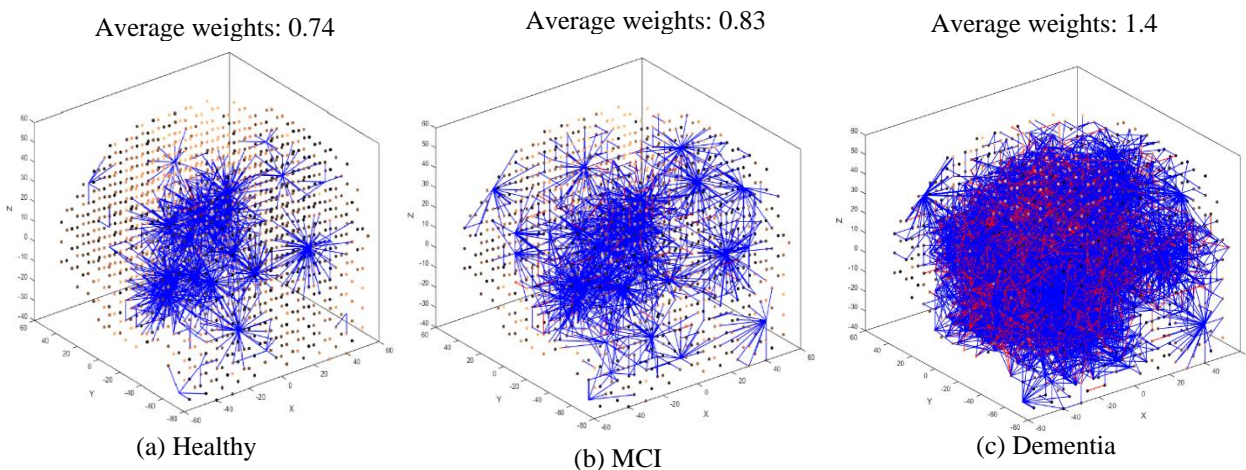


Figure 10. Personalised profiling of three randomly selected individuals from H (shown in a) MCI (shown in b) and dementia (shown in c) groups. These three PSNN models are trained with the use of spike trains of different KNN samples of MRI data for each individual. The spatiotemporal *connectivity* in a PSNN model of an individual from the dementia group (in c) illustrates more connections when compared with the models of the H individual (in a). The enhanced SNN *connectivity* in the individual diagnosed with dementia is due to an increased amount of changes in the values of certain MRI features in this patient over the period of follow-up. These MRI changes were encoded into more spikes, causing enhanced connections during the PSNN model's learning process. The blue lines are positive (excitatory) connections, while the red lines are negative (inhibitory) connections. The thickness of the lines identifies the weight of the connections.

This section demonstrated that the computational SNN models for personalised modelling of longitudinal MRI data were created to perform pattern recognition, classification, and prediction of cognitive outcomes (healthy, MCI and dementia). The models demonstrated the spatiotemporal interactions (in the form of connections) between the MRI features in a computational SNN model, rather than an exact structure of the brain's physical neural *connectivity*. The SNN models learned from the changes in MRI time series which were encoded into spikes. The learning was performed using STDP, which changes the synaptic strength based on the difference in firing time of pre- and postsynaptic *neurons*. Using an encoding method, drastic changes in MRI data were encoded to more positive or negative spikes. The greater intensity of these input spikes and their propagation to the SNN model caused more repeated spike transformation between the *neurons* during the STDP. Therefore, the absolute values of the

connection weights (both positive and negative) increased over time. This means that greater spatiotemporal connections in the SNN models represent more changes in the MRI time series. Our findings presented that the SNN model of dementia group has stronger changes across several brain regions, demonstrated in the form of spatiotemporal *connections* in the SNN model. The SNN models were also used for classification and prediction of cognitive outcomes when tested with a new MRI sample. The models were able to accurately classify and predict 2-year ahead of cognitive decline (MCI and dementia) with 96% and 90% accuracy respectively, which were better than the accuracy from traditional classifiers.

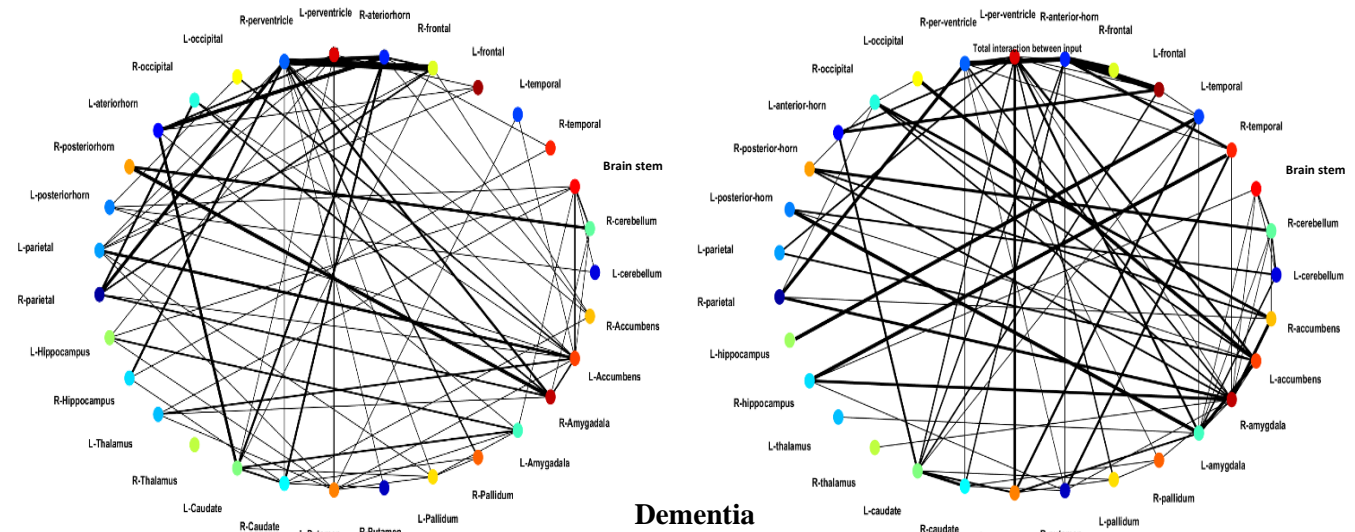
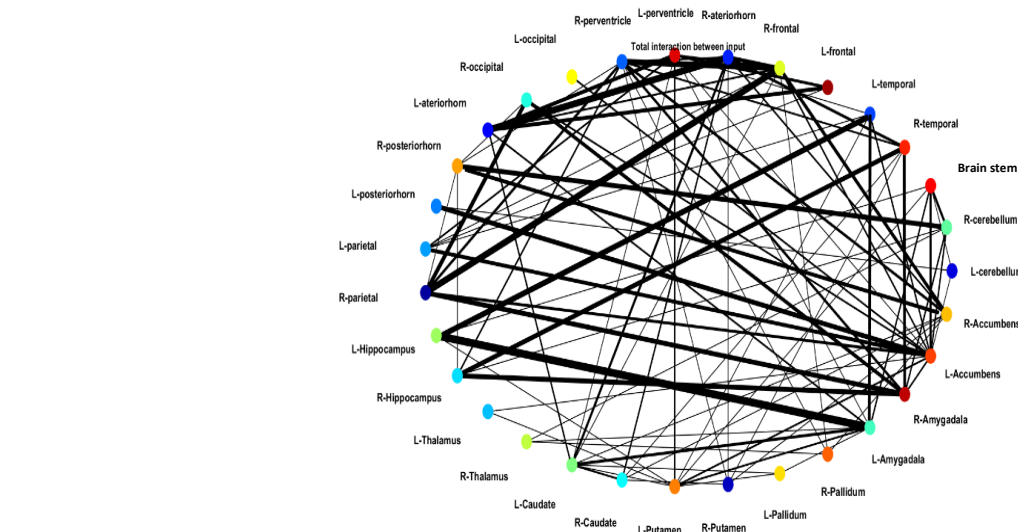
Healthy**MCI****Dementia**

Figure 11. The FIN graphs that show the causal, temporal relationship between the longitudinal changes in MRI features over 6-year period of follow-up for three individuals, randomly selected from the participants who developed to MCI or dementia, or remained healthy after 6 years (labels are from the last follow-up assessment). The thicker the line, the more temporal interactions between the features (brain areas) over the period of 6 years have been captured in the PSNN model. A FIN graph allows us to discover and investigate the functionality of interacting brain areas for each of the 3 outcome groups.

4. Discussion

The MRI modelling in this research suggested certain regional changes in WMH and structural volume associated with MCI and dementia development over 6 years. The results in Figs. 6 and 9 demonstrated left-right asymmetry in SNN *connectivity* in certain brain areas, particularly presented in the cerebellum, temporal, occipital and parietal as well as in periventricular areas while this asymmetry was less presented in the MCI and H groups. A relevant finding was previously reported for hippocampal volumes asymmetry during the progression of Alzheimer's disease [20].

Our findings in Fig. 6 demonstrated that the MRI changes over 6 years in frontal and parietal lobes diverged considerably between healthy, MCI, and dementia groups and would, therefore, be potential markers for predicting cognitive outcomes. Significant changes from time T1 to T4 are seen in dementia more than in MCI. This finding supports the results of another study which reported MCI is correlated to structural vulnerability and differential volume change across brain regions [94]. The results from the current study are also aligned with previous research that reported alterations in different brain regions, as Zidan et al [95] who found that volumes in the hippocampus are lower in people with Alzheimer's disease compared to individuals with MCI. Also, Gootjes et al [96] showed that the WMH index (WMH volume separated by lobar volume) was greater in people with dementia while it was at a low level in healthy controls and, within each group, the WMH index was elevated more in parietal and frontal lobes than in temporal and occipital lobes.

Based on the encoding algorithm, drastic changes in MRI data over time (both increases and decreases) leads to the generation of a greater number of spikes (both positive and negative), which are then entered into the SNN model for the learning process. According to the LIF model of a spiking *neuron*, if a *neuron* receives more frequent input spikes over time, its potential increases faster and generates more frequent output spikes. The STDP rule changes the synaptic strength based on the difference in firing time of pre- and postsynaptic *neurons*. The greater intensity of these input spikes and their propagation to the SNN model caused more repeated spike exchange between the *neurons* during the STDP. Therefore, the absolute values of the connection weights (both positive and negative) increased over time. This means that greater spatiotemporal connections in the SNN models represent more changes in the MRI time series. The created computational SNN models in Fig. 8 were trained by 6 years of MRI time series from healthy, MCI and dementia groups. The findings suggested that the model of dementia has shown stronger connections (average connection weights= 1.1) across several areas when compared with the models of H (average connection weights= 0.93) and MCI (average connection weights= 0.81). The quantitative information of the SNN models (shown in Fig. 9) demonstrated that dementia group had much stronger connection weights in some brain regions, such as the right cerebellum, left temporal, right frontal, right occipital, right posterior horn, right parietal, and right amygdala. These connections were developed during the STDP learning with spike trains of interpolated MRI data.

FINs in Fig. 11 depicted networks of interactions between MRI features over 6 years and demonstrated the changes in one MRI feature caused some changes in other ones. Compared to the healthy control group, interactions are stronger in the FINs of MCI and much stronger in the dementia group. This represents greater brain changes were captured during the 6 years of follow-up for individuals with dementia. For example, in Fig. 11, the FIN of MCI demonstrated stronger interactions between the volume changes in left and right hippocampus and the WMH of the temporal region. These cognitive changes were shown to be enhanced across several brain regions in the FIN of the dementia group which demonstrated strong associations between the changes in the volumes of the amygdala, hippocampus and WMH of temporal and posterior horn regions. Our finding is consistent with previous research on hippocampus and amygdala atrophy in relation to cognitive decline [97]. Furthermore, other studies report an association of WMH with the risk of progressing from healthy ageing to MCI [18] and the regional specificity of the association of WMH with cognitive functions, memory performance and Alzheimer's disease [19, 98].

Brickman et al also indicated that WMH volume in the parietal lobe predicts incidents of dementia while in people with Parkinson disease, the hippocampal volume is a main component in predicting MCI and dementia [20].

SNNs in principle are excellent tools to understand changes in multivariate spatiotemporal data and memorise them in their connections [99]. Furthermore, this SNN is structured according to a brain template so that the learnt connections can be interpreted to understand and discover markers of changes in the brain data over time related to certain outcomes. The proposed personalised modelling using SNN allows for capturing the relationship between the MRI features in the form of spatiotemporal *connectivity* in relation to the outputs. Therefore, the model does not act as a black-box information processing system, but as an interpretable model that demonstrates what interactions between the features have triggered the output. In contrast to our proposed approach, the current deep learning methods, such as CNN, have no brain-like structured architecture to learn both time and space components of longitudinal brain data in one unifying model. Knowledge discovery in deep-learning patterns generated during the learning time, in an unsupervised mode in SNN models, from spatiotemporal data streams is of crucial importance for the interpretability. In the current study this has allowed for a better interpretation of the spatiotemporal interactions between variables when compared with black-box conventional classifiers and statistical methods such as SVM, MLP and MLR.

Although there are neuroimaging studies that investigated and reported association of longitudinal brain changes with the risk of progression from normal cognitive conditions to MCI and dementia [18, 95, 100], personalised neuroimaging data modelling for accurate classification and prediction of individual cognitive outcomes in older people is still lacking. Our proposed methodology aims to solve a challenging problem of how to integrate diverse brain changes that occur spatially and over time (as measured with MRI), into the comprehensive predictive algorithm. Future directions include:

- Applying the proposed methodology on larger data cohorts.
- Applying the personalised modelling system to the larger number of features in the same cohort, such as clinical and psychometric assessments that may provide complementary information and lead to improve the accuracy of classification and prediction of brain changes associated with various cognitive outcomes. This will help to better understand the processes underlying the development of neurodegenerative and cerebrovascular diseases.
- Developing new deep learning algorithms to complement the existing ones.
- Developing new algorithms for symbolic spatiotemporal rule extraction from trained PSNN to better understand individual brain dynamics related to outcomes.
- Implementation of diagnostic tools for clinical practice.

5. Conclusion

The current study introduces a new method for personalised predictive modelling of longitudinal data using a brain-inspired SNN architecture for early prediction and classification of neurological state (healthy, MCI and dementia). The novel methods were applied to longitudinal (across 6 years) MRI data from the Sydney MAS study (Australia), which represents a reliable cohort of older adults.

The proposed methodology consists of several procedures, including: data imputation to deal with missing values, data interpolation to transfer longitudinal MRI data to time series; encoding the MRI time series into sequences of spikes that represent significant data changes over time; mapping the MRI data into 3-dimensional brain-inspired SNN model structured according to a brain template; unsupervised and supervised training from the MRI data; classifying/predicting an individual cognitive conditions with superior accuracy to traditional machine learning

classifiers; visualisation and interpretation of results for individual marker discovery. The methodology used in this paper is based on a brain-inspired SNN architecture and has several advantages compared to traditional machine learning methods, including:

- High accuracy and sensitivity of an individual cognitive outcome classification and prediction. The SNN models were able to predict 2 years ahead of cognitive declines (MCI and dementia) with 90% accuracy.
- Enabling the creation of individual models for a better understanding of changes in an individual's longitudinal MRI data over time, representing an individual cognitive degeneration.

Acknowledgements

The data from the Memory and Ageing Study (MAS) were provided by the MAS Management Committee. This research was supported by a research grant from the Brain Research New Zealand Centre of Research Excellence (BRNZ CoRE) and by the AUT SRIF Interact funding of the Knowledge Engineering & Discovery Research Institute (KEDRI) in collaboration with the National Institute for Stroke and Applied Neurosciences (NISAN) of Auckland University of Technology, New Zealand. The authors would like to sincerely acknowledge the support from Donna Rose Addis (Rotman Research Institute, University of Toronto), Anbupalam Thalamuthu (Centre for Healthy Brain Ageing, School of Psychiatry, University of New South Wales, Sydney, Australia) and Lynette Tippet (School of Psychology, Centre for Brain Research, University of Auckland, and Brain Research New Zealand) and Prof Edmund Lai (Auckland University of Technology).

Contribution of Authors

- Maryam Doborjeh conducted literature search, participated in the design of the study, conducted system implementations, performed the experiments, conducted data analysis and interpretation, authored and reviewed drafts of the paper, prepared figures and/or tables, approved the final draft, submitted the manuscript.
- Zohreh Doborjeh participated in the design of the methods, experimental design, conducted data analysis, statistical analysis of the results and interpretation, prepared figures, and tables, authored and reviewed drafts of the paper, approved the final draft.
- Alexander Merkin completed literature search, conducted data analysis and data interpretation, authored or reviewed drafts of the paper, approved the final draft.
- Helena Bahrami developed study design, conducted data analysis and interpretation, authored and reviewed drafts of the paper, prepared figures and/or tables, approved the final draft.
- Alex Sumich performed statistical analysis, interpretation of results, reviewed drafts of the paper, approved the final draft.
- Oleg N. Medvedev conducted data analysis and interpretation, reviewed drafts of the paper, approved the final draft.
- Mark Crook-Rumsey conducted data analysis and interpretation, reviewed drafts of the paper, approved and proofread the final draft.
- Kristan Kang completed data collection, conducted data analysis and interpretation, authored or reviewed drafts of the paper, approved the final draft.
- Catherine Morgan conducted data analysis and interpretation, reviewed drafts of the paper, approved the final draft.
- Ian Kirk participated in the data analysis and interpretation of results, approved the final draft.

- 816 • Perminder Sachdev provided the MAS data and its explanation, reviewed drafts of the paper, and approved the
817 final draft.
- 818 • Henry Brodaty provided the MAS data and its explanation, reviewed manuscript drafts and approved the final
819 draft.
- 820 • Wei Wen provided the MAS data and its explanation, reviewed drafts of the paper, and approved the final draft.
- 821 • Rita Krishnamurthi reviewed the manuscript draft, contributed to the interpretation of the results, and approved
822 the final draft.
- 823 • Valery Feigin led the project and participated in the data analysis and interpretation of results, reviewed drafts
824 of the paper, approved the final draft.
- 825 • Nikola Kasabov led the design of the SNN architecture and methodology, authored and reviewed drafts of the
826 paper, approved the final draft.
- 827

828 Declaration of Interest

829 The authors declare that they have no known competing financial interests or personal relationships that could have
830 appeared to influence the work reported in this paper.

831 Ethical Approval

832 The data recording was approved by Committees of the University of New South Wales and the South Eastern
833 Sydney and Illawarra Area Health Service. In New Zealand, the Ethics Approval for the study was reviewed by the
834 Auckland University of Technology Ethics Committee (AUTEK), and ethical approval has been granted for three
835 years until 1 March 2021.

836 Data Availability Statement

837 The terms of consent for research participation stipulate that an individual's data can only be shared outside of the
838 MAS investigators group if the group has reviewed and approved the proposed secondary use of the data. This
839 consent applies regardless of whether data has been de-identified. Access is mediated via a standardised request
840 process managed by the CHeBA Research Bank, who can be contacted at ChebaData@unsw.edu.au or via the first
841 author's contact at mgholami@aut.ac.nz.

842

843 References

- 844 [1] G. A. Wellenius *et al.*, "Ambient air pollution and the risk of acute ischemic stroke," *Archives of internal medicine*,
845 vol. 172, no. 3, pp. 229-234, 2012.
- 846 [2] G. Livingston *et al.*, "Dementia prevention, intervention, and care," *The Lancet*, Article in Press pp. DOI:
847 10.1016/S0140-6736(17)31363-6, 2017, doi: 10.1016/S0140-6736(17)31363-6.
- 848 [3] G. Rait *et al.*, "Prevalence of cognitive impairment: Results from the MRC trial of assessment and management of
849 older people in the community," *Age and Ageing*, Article vol. 34, no. 3, pp. 242-248, 2005, doi: 10.1093/ageing/afi039.
- 850 [4] A. Ward, H. M. Arrighi, S. Michels, and J. M. Cedarbaum, "Mild cognitive impairment: Disparity of incidence and
851 prevalence estimates," *Alzheimer's and Dementia*, Article vol. 8, no. 1, pp. 14-21, 2012, doi:
852 10.1016/j.jalz.2011.01.002.
- 853 [5] H. Brodaty *et al.*, "Operationalizing the diagnostic criteria for mild cognitive impairment: the salience of objective
854 measures in predicting incident dementia," *The American Journal of Geriatric Psychiatry*, vol. 25, no. 5, pp. 485-497,
855 2017.

- 856 [6] K. Palmer, L. Backman, B. Winblad, and L. Fratiglioni, "Mild cognitive impairment in the general population:
857 Occurrence and progression to alzheimer disease," *American Journal of Geriatric Psychiatry*, Article vol. 16, no. 7,
858 pp. 603-611, 2008, doi: 10.1097/JGP.0b013e3181753a64.
- 859 [7] K. Palmer, A. K. Berger, R. Monastero, B. Winblad, L. Bäckman, and L. Fratiglioni, "Predictors of progression from
860 mild cognitive impairment to Alzheimer disease," *Neurology*, Article vol. 68, no. 19, pp. 1596-1602, 2007, doi:
861 10.1212/01.wnl.0000260968.92345.3f.
- 862 [8] L. Aerts *et al.*, "Effects of MCI subtype and reversion on progression to dementia in a community sample," *Neurology*,
863 Article vol. 88, no. 23, pp. 2225-2232, 2017, doi: 10.1212/WNL.0000000000004015.
- 864 [9] F. E. Matthews *et al.*, "A two decade dementia incidence comparison from the Cognitive Function and Ageing Studies
865 I and II," *Nature communications*, vol. 7, no. 1, pp. 1-8, 2016.
- 866 [10] P. Thompson *et al.*, "Cortical variability and asymmetry in normal aging and Alzheimer's disease," *Cerebral Cortex*
867 (*New York, NY: 1991*), vol. 8, no. 6, pp. 492-509, 1998.
- 868 [11] C. Yang, S. Zhong, X. Zhou, L. Wei, L. Wang, and S. Nie, "The abnormality of topological asymmetry between
869 hemispheric brain white matter networks in Alzheimer's disease and mild cognitive impairment," *Frontiers in aging*
870 *neuroscience*, vol. 9, p. 261, 2017.
- 871 [12] D. Chen *et al.*, "Brain network and abnormal hemispheric asymmetry analyses to explore the marginal differences in
872 glucose metabolic distributions among Alzheimer's Disease, Parkinson's Disease Dementia, and Lewy Body
873 Dementia," *Frontiers in neurology*, vol. 10, p. 369, 2019.
- 874 [13] C. Wachinger, D. H. Salat, M. Weiner, M. Reuter, and A. s. D. N. Initiative, "Whole-brain analysis reveals increased
875 neuroanatomical asymmetries in dementia for hippocampus and amygdala," *Brain*, vol. 139, no. 12, pp. 3253-3266,
876 2016.
- 877 [14] B. Cholerteron *et al.*, "Precision Medicine: Clarity for the Complexity of Dementia," (in eng), *Am J Pathol*, vol. 186,
878 no. 3, pp. 500-6, Mar 2016, doi: 10.1016/j.ajpath.2015.12.001.
- 879 [15] S. Spasov, L. Passamonti, A. Duggento, P. Liò, N. Toschi, and A. s. D. N. Initiative, "A parameter-efficient deep
880 learning approach to predict conversion from mild cognitive impairment to Alzheimer's disease," *Neuroimage*, vol.
881 189, pp. 276-287, 2019.
- 882 [16] A. A. Willette, V. D. Calhoun, J. M. Egan, D. Kapogiannis, and A. s. D. N. Initiative, "Prognostic classification of
883 mild cognitive impairment and Alzheimer' s disease: MRI independent component analysis," *Psychiatry Research:*
884 *Neuroimaging*, vol. 224, no. 2, pp. 81-88, 2014.
- 885 [17] E. M. Reiman *et al.*, "Exceptionally low likelihood of Alzheimer's dementia in APOE2 homozygotes from a 5,000-
886 person neuropathological study," *Nature Communications*, vol. 11, no. 1, pp. 1-11, 2020.
- 887 [18] E. E. Smith *et al.*, "Magnetic resonance imaging white matter hyperintensities and brain volume in the prediction of
888 mild cognitive impairment and dementia," *Archives of neurology*, vol. 65, no. 1, pp. 94-100, 2008.
- 889 [19] A. M. Brickman *et al.*, "Regional white matter hyperintensity volume, not hippocampal atrophy, predicts incident
890 Alzheimer disease in the community," *Archives of neurology*, vol. 69, no. 12, pp. 1621-1627, 2012.
- 891 [20] J. Barnes, R. I. Scahill, J. M. Schott, C. Frost, M. N. Rossor, and N. C. Fox, "Does Alzheimer's disease affect
892 hippocampal asymmetry? Evidence from a cross-sectional and longitudinal volumetric MRI study," *Dementia and*
893 *geriatric cognitive disorders*, vol. 19, no. 5-6, pp. 338-344, 2005.
- 894 [21] I. S. Van Maurik *et al.*, "Interpreting biomarker results in individual patients with mild cognitive impairment in the
895 Alzheimer's biomarkers in daily practice (ABIDE) project," *JAMA neurology*, vol. 74, no. 12, pp. 1481-1491, 2017.
- 896 [22] N. Franzmeier *et al.*, "Functional brain architecture is associated with the rate of tau accumulation in Alzheimer's
897 disease," *Nature Communications*, vol. 11, no. 1, pp. 1-17, 2020.
- 898 [23] S. E. Harris *et al.*, "Neurology-related protein biomarkers are associated with cognitive ability and brain volume in
899 older age," *Nature Communications*, vol. 11, no. 1, pp. 1-12, 2020.
- 900 [24] M. Khalil *et al.*, "Serum neurofilament light levels in normal aging and their association with morphologic brain
901 changes," *Nature Communications*, vol. 11, no. 1, pp. 1-9, 2020.
- 902 [25] A. M. Nicholson *et al.*, "Prosaposin is a regulator of progranulin levels and oligomerization," *Nature communications*,
903 vol. 7, no. 1, pp. 1-14, 2016.
- 904 [26] M. Canevelli *et al.*, "Spontaneous Reversion of Mild Cognitive Impairment to Normal Cognition: A Systematic
905 Review of Literature and Meta-Analysis," *Journal of the American Medical Directors Association*, Article vol. 17,
906 no. 10, pp. 943-948, 2016, doi: 10.1016/j.jamda.2016.06.020.
- 907 [27] A. S. Lundervold and A. Lundervold, "An overview of deep learning in medical imaging focusing on MRI," *Zeitschrift*
908 *für Medizinische Physik*, vol. 29, no. 2, pp. 102-127, 2019.
- 909 [28] A. Benou, R. Veksler, A. Friedman, and T. R. Raviv, "Ensemble of expert deep neural networks for spatio-temporal
910 denoising of contrast-enhanced MRI sequences," *Medical image analysis*, vol. 42, pp. 145-159, 2017.

- 911 [29] C. Bermudez, A. J. Plassard, L. T. Davis, A. T. Newton, S. M. Resnick, and B. A. Landman, "Learning implicit brain
912 MRI manifolds with deep learning," in *Medical Imaging 2018: Image Processing*, 2018, vol. 10574: International
913 Society for Optics and Photonics, p. 105741L.
- 914 [30] T. Küstner *et al.*, "Automated reference-free detection of motion artifacts in magnetic resonance images," *Magnetic
915 Resonance Materials in Physics, Biology and Medicine*, vol. 31, no. 2, pp. 243-256, 2018.
- 916 [31] K. Zeng, H. Zheng, C. Cai, Y. Yang, K. Zhang, and Z. Chen, "Simultaneous single-and multi-contrast super-resolution
917 for brain MRI images based on a convolutional neural network," *Computers in biology and medicine*, vol. 99, pp. 133-
918 141, 2018.
- 919 [32] M. Cabezas, A. Oliver, X. Lladó, J. Freixenet, and M. B. Cuadra, "A review of atlas-based segmentation for magnetic
920 resonance brain images," *Computer methods and programs in biomedicine*, vol. 104, no. 3, pp. e158-e177, 2011.
- 921 [33] J. Schmidhuber, "Deep learning in neural networks: An overview," *Neural networks*, vol. 61, pp. 85-117, 2015.
- 922 [34] L. Chen, P. Bentley, and D. Rueckert, "Fully automatic acute ischemic lesion segmentation in DWI using
923 convolutional neural networks," *NeuroImage: Clinical*, vol. 15, pp. 633-643, 2017.
- 924 [35] M. Havaei *et al.*, "Brain tumor segmentation with deep neural networks," *Medical image analysis*, vol. 35, pp. 18-31,
925 2017.
- 926 [36] E. A. AlBadawy, A. Saha, and M. A. Mazurowski, "Deep learning for segmentation of brain tumors: Impact of cross-
927 institutional training and testing," *Medical physics*, vol. 45, no. 3, pp. 1150-1158, 2018.
- 928 [37] J. Islam and Y. Zhang, "Brain MRI analysis for Alzheimer's disease diagnosis using an ensemble system of deep
929 convolutional neural networks," *Brain informatics*, vol. 5, no. 2, p. 2, 2018.
- 930 [38] A. Gupta, M. Ayhan, and A. Maida, "Natural image bases to represent neuroimaging data," in *International
931 conference on machine learning*, 2013, pp. 987-994.
- 932 [39] D. Lu, K. Popuri, G. W. Ding, R. Balachandar, and M. F. Beg, "Multimodal and multiscale deep neural networks for
933 the early diagnosis of Alzheimer's disease using structural MR and FDG-PET images," *Scientific reports*, vol. 8, no.
934 1, pp. 1-13, 2018.
- 935 [40] A. L. Hodgkin, A. F. Huxley, and B. Katz, "Measurement of Current-Voltage Relations in the Membrane of the Giant
936 Axon of Loligo," *The Journal of Physiology*, vol. 116, no. 4, pp. 424-448, 1952.
- 937 [41] J. E. Hall, *Guyton and Hall Textbook of Medical Physiology e-Book*. Elsevier Health Sciences, 2015.
- 938 [42] W. Maass, "Networks of spiking neurons: the third generation of neural network models," *Neural networks*, vol. 10,
939 no. 9, pp. 1659-1671, 1997.
- 940 [43] E. M. Izhikevich, "Polychronization: Computation with Spikes," *Neural Computation*, vol. 18, no. 2, pp. 245-282,
941 2006.
- 942 [44] R. Brette *et al.*, "Simulation of Networks of Spiking Neurons: A Review of Tools and Strategies," *Journal of
943 Computational Neuroscience*, vol. 23, no. 3, pp. 349-398, 2007.
- 944 [45] N. Scott, N. Kasabov, and G. Indiveri, "NeuCube Neuromorphic Framework for Spatio-temporal Brain Data and Its
945 Python Implementation," in *Neural Information Processing*: Springer, 2013, pp. 78-84.
- 946 [46] S. Thorpe and J. Gautrais, "Rank Order Coding," in *Computational Neuroscience*: Springer, 1998, pp. 113-118.
- 947 [47] D. Verstraeten, B. Schrauwen, M. D'Haene, and D. Stroobandt, "An Experimental Unification of Reservoir
948 Computing Methods," *Neural Networks*, vol. 20, no. 3, pp. 391-403, 2007.
- 949 [48] T. Masquelier, R. Guyonneau, and S. Thorpe, "Competitive STDP-based Spike Pattern Learning," *Neural
950 Computation*, vol. 21, no. 5, pp. 1259-1276, 2009.
- 951 [49] N. Caporale and Y. Dan, "Spike timing-dependent plasticity: a Hebbian learning rule," *Annu. Rev. Neurosci.*, vol. 31,
952 pp. 25-46, 2008.
- 953 [50] R. C. Froemke, M.-m. Poo, and Y. Dan, "Spike-timing-dependent synaptic plasticity depends on dendritic location,"
954 *Nature*, vol. 434, no. 7030, pp. 221-225, 2005.
- 955 [51] B. L. McNaughton and R. G. Morris, "Hippocampal synaptic enhancement and information storage within a
956 distributed memory system," *Trends in neurosciences*, vol. 10, no. 10, pp. 408-415, 1987.
- 957 [52] A. Treves and E. T. Rolls, "Computational analysis of the role of the hippocampus in memory," *Hippocampus*, vol. 4,
958 no. 3, pp. 374-391, 1994.
- 959 [53] F. Zenke, E. J. Agnes, and W. Gerstner, "Diverse synaptic plasticity mechanisms orchestrated to form and retrieve
960 memories in spiking neural networks," *Nature communications*, vol. 6, no. 1, pp. 1-13, 2015.
- 961 [54] D. E. Feldman, "The spike-timing dependence of plasticity," *Neuron*, vol. 75, no. 4, pp. 556-571, 2012.
- 962 [55] C. Clopath, L. Büsing, E. Vasilaki, and W. Gerstner, "Connectivity reflects coding: a model of voltage-based STDP
963 with homeostasis," *Nature neuroscience*, vol. 13, no. 3, p. 344, 2010.
- 964 [56] S. Valtcheva and L. Venance, "Astrocytes gate Hebbian synaptic plasticity in the striatum," *Nature communications*,
965 vol. 7, no. 1, pp. 1-17, 2016.

- [57] B. Cramer *et al.*, "Control of criticality and computation in spiking neuromorphic networks with plasticity," *Nature Communications*, vol. 11, no. 1, pp. 1-11, 2020.
- [58] J. C. Magee and D. Johnston, "A synaptically controlled, associative signal for Hebbian plasticity in hippocampal neurons," *Science*, vol. 275, no. 5297, pp. 209-213, 1997.
- [59] P. S. Sachdev *et al.*, "The Sydney Memory and Ageing Study (MAS): methodology and baseline medical and neuropsychiatric characteristics of an elderly epidemiological non-demented cohort of Australians aged 70-90 years," (in eng), *International psychogeriatrics*, vol. 22, no. 8, pp. 1248-64, Dec 2010, doi: 10.1017/s1041610210001067.
- [60] S. American Psychiatric Association Committee on Nomenclature and, *Diagnostic and Statistical Manual of Mental Disorders (DSM-IV)*. Washington, DC: American Psychiatric Association, 1994.
- [61] A. Yendiki. "FreeSurfer." <https://surfer.nmr.mgh.harvard.edu/fswiki> (accessed 15/06/2020, 2020).
- [62] J. Jiang *et al.*, "UBO Detector—A cluster-based, fully automated pipeline for extracting white matter hyperintensities," *Neuroimage*, vol. 174, pp. 539-549, 2018.
- [63] S. Song, K. D. Miller, and L. F. Abbott, "Competitive Hebbian learning through spike-timing-dependent synaptic plasticity," *Nature neuroscience*, vol. 3, no. 9, p. 919, 2000.
- [64] N. Kasabov, "Global, local and personalised modeling and pattern discovery in bioinformatics: An integrated approach," *Pattern Recognition Letters*, vol. 28, no. 6, pp. 673-685, 2007.
- [65] B. Petro, N. Kasabov, and R. M. Kiss, "Selection and optimization of temporal spike encoding methods for spiking neural networks," *IEEE transactions on neural networks and learning systems*, 2019.
- [66] K. Dhoble, N. Nuntalid, G. Indiveri, and N. Kasabov, "Online spatio-temporal pattern recognition with evolving spiking neural networks utilising address event representation, rank order, and temporal spike learning," in *IEEE World Congress on Computational Intelligence*, Brisbane, Australia, 2012, pp. 1-7.
- [67] B. Schrauwen and J. Van Campenhout, "BSA, a fast and accurate spike train encoding scheme," in *Proceedings of the international joint conference on neural networks*, 2003, vol. 4: IEEE Piscataway, NJ, pp. 2825--2830.
- [68] S. M. Bohte, "The evidence for neural information processing with precise spike-times: A survey," *Natural Computing*, vol. 3, no. 2, pp. 195-206, 2004.
- [69] E. R. Kandel *et al.*, *Principles of neural science*. McGraw-hill New York, 2000.
- [70] E. M. Izhikevich, "Simple Model of Spiking Neurons," *IEEE Transactions on neural networks*, vol. 14, no. 6, pp. 1569-1572, 2003.
- [71] E. Bullmore and O. Sporns, "Complex brain networks: graph theoretical analysis of structural and functional systems," *Nature reviews neuroscience*, vol. 10, no. 3, p. 186, 2009.
- [72] V. Braitenberg and A. Schüz, *Cortex: statistics and geometry of neuronal connectivity*. Springer Science & Business Media, 2013.
- [73] J. DeFelipe, "Neocortical neuronal diversity: chemical heterogeneity revealed by colocalization studies of classic neurotransmitters, neuropeptides, calcium-binding proteins, and cell surface molecules," *Cerebral cortex*, vol. 3, no. 4, pp. 273-289, 1993.
- [74] L. F. Abbott, "Lapicque's introduction of the integrate-and-fire model neuron (1907)," *Brain research bulletin*, vol. 50, no. 5-6, pp. 303-304, 1999.
- [75] B. W. Knight, "Dynamics of encoding in a population of neurons," *The Journal of general physiology*, vol. 59, no. 6, pp. 734-766, 1972.
- [76] F. Ponulak and A. Kasinski, "Introduction to spiking neural networks: Information processing, learning and applications," *Acta neurobiologiae experimentalis*, vol. 71, no. 4, pp. 409-433, 2011.
- [77] W. Gerstner, W. M. Kistler, R. Naud, and L. Paninski, *Neuronal dynamics: From single neurons to networks and models of cognition*. Cambridge University Press, 2014.
- [78] Y. Dan and M.-M. Poo, "Spike timing-dependent plasticity: from synapse to perception," *Physiological reviews*, vol. 86, no. 3, pp. 1033-1048, 2006.
- [79] N. Kasabov, K. Dhoble, N. Nuntalid, and G. Indiveri, "Dynamic evolving spiking neural networks for on-line spatio-temporal pattern recognition," *Neural Networks*, vol. 41, pp. 188-201, 2013.
- [80] S. Thorpe and J. Gautrais, "Rank order coding," in *Computational Neuroscience*, 1998: Springer, pp. 113-118.
- [81] D. R. Kunkle and C. Merrigan, "Pulsed neural networks and their application," *Computer Science Dept., College of Computing and Information Sciences, Rochester Institute of Technology*, 2002.
- [82] J. Vreeken, "Spiking neural networks, an introduction," ed: Utrecht University: Information and Computing Sciences, 2003.
- [83] A. Calimera, E. Macii, and M. Poncino, "The human brain project and neuromorphic computing," *Functional neurology*, vol. 28, no. 3, p. 191, 2013.
- [84] D. Monroe, "Neuromorphic computing gets ready for the (really) big time," ed: ACM New York, NY, USA, 2014.

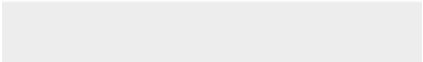

- 1021 [85] J. Talairach, "Co-planar stereotaxic atlas of the human brain-3-dimensional proportional system," *An approach to*
 1022 *cerebral imaging*, 1988.
- 1023 [86] A. R. Laird, J. J. Lancaster, and P. T. Fox, "Brainmap," *Neuroinformatics*, vol. 3, no. 1, pp. 65-77, 2005.
- 1024 [87] J. L. Lancaster *et al.*, "Automated Talairach atlas labels for functional brain mapping," *Human brain mapping*, vol.
 1025 10, no. 3, pp. 120-131, 2000.
- 1026 [88] L. Koessler *et al.*, "Automated cortical projection of EEG sensors: anatomical correlation via the international 10–10
 1027 system," *Neuroimage*, vol. 46, no. 1, pp. 64-72, 2009.
- 1028 [89] K. Brodmann, *Vergleichende Lokalisationslehre der Grosshirnrinde in ihren Prinzipien dargestellt auf Grund des*
 1029 *Zellenbaues*. Barth, 1909.
- 1030 [90] A. Field, *Discovering statistics using IBM SPSS statistics*. SAGE, 2013.
- 1031 [91] H. Han, W.-Y. Wang, and B.-H. Mao, "Borderline-SMOTE: a new over-sampling method in imbalanced data sets
 1032 learning," in *International conference on intelligent computing*, 2005: Springer, pp. 878-887.
- 1033 [92] D. S. Bassett and E. T. Bullmore, "Small-world brain networks revisited," *The Neuroscientist*, vol. 23, no. 5, pp. 499-
 1034 516, 2017.
- 1035 [93] F. K. Došilović, M. Brčić, and N. Hlupić, "Explainable artificial intelligence: A survey," in *2018 41st International*
 1036 *convention on information and communication technology, electronics and microelectronics (MIPRO)*, 2018: IEEE,
 1037 pp. 0210-0215.
- 1038 [94] I. Driscoll *et al.*, "Longitudinal pattern of regional brain volume change differentiates normal aging from MCI,"
 1039 *Neurology*, vol. 72, no. 22, pp. 1906-1913, 2009.
- 1040 [95] M. Zidan *et al.*, "Thalamic volume loss as an early sign of amnesic mild cognitive impairment," (in eng), *Journal of*
 1041 *clinical neuroscience : official journal of the Neurosurgical Society of Australasia*, vol. 68, pp. 168-173, Oct 2019,
 1042 doi: 10.1016/j.jocn.2019.07.004.
- 1043 [96] L. Gootjes *et al.*, "Regional distribution of white matter hyperintensities in vascular dementia, Alzheimer's disease
 1044 and healthy aging," *Dementia and geriatric cognitive disorders*, vol. 18, no. 2, pp. 180-188, 2004.
- 1045 [97] L. Yue *et al.*, "Asymmetry of hippocampus and amygdala defect in subjective cognitive decline among the community
 1046 dwelling Chinese," *Frontiers in psychiatry*, vol. 9, p. 226, 2018.
- 1047 [98] I. B. Meier *et al.*, "White matter predictors of cognitive functioning in older adults," (in eng), *Journal of the*
 1048 *International Neuropsychological Society : JINS*, vol. 18, no. 3, pp. 414-27, May 2012, doi:
 1049 10.1017/s1355617712000227.
- 1050 [99] N. K. Kasabov, *Time-space, spiking neural networks and brain-inspired artificial intelligence*. Springer, 2019.
- 1051 [100] B. Dickerson *et al.*, "Alzheimer-signature MRI biomarker predicts AD dementia in cognitively normal adults,"
 1052 *Neurology*, vol. 76, no. 16, pp. 1395-1402, 2011.

1053



[Click here to access/download](#)

Supplementary Material for on-line publication only
Supplementary.pdf



Declaration of interests

☒ The authors declare that they have no known competing financial interests or personal relationships that could have appeared to influence the work reported in this paper.

☐The authors declare the following financial interests/personal relationships which may be considered as potential competing interests: